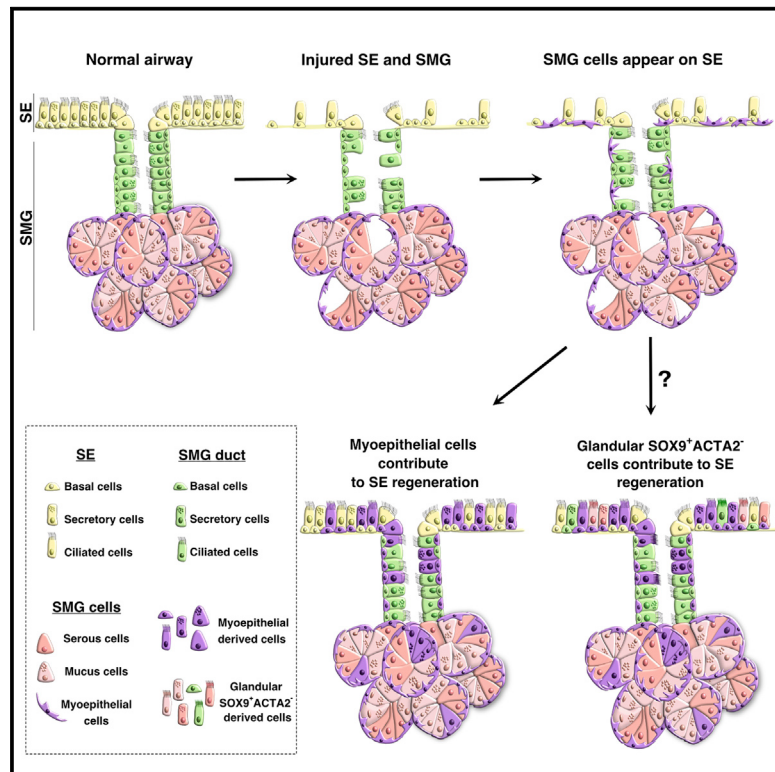


Myoepithelial Cells of Submucosal Glands Can Function as Reserve Stem Cells to Regenerate Airways after Injury

Graphical Abstract



Authors

Aleksandra Tata, Yoshihiko Kobayashi, Ryan D. Chow, ..., Timothy J. McCord, Michael Dee Gunn, Purushothama Rao Tata

Correspondence

purushothamarao.tata@duke.edu

In Brief

Airway submucosal glands are reservoirs of mucous and anti-microbial products that provide defense against microbes. Here, Tata and colleagues uncover a hidden reserve multipotent stem cell population in SMGs that can proliferate, migrate, and transdifferentiate to repair surface epithelium following injury through a SOX9-dependent transcriptional program.

Highlights

- SMGs harbor reserve multipotent stem cells that can contribute to SE repair
- MECs contribute to both basal and luminal cells of the SMGs and SE after injury
- SMG-like cells are found on porcine SE following severe airway injury
- SOX9-dependent mechanisms drive MECs proliferation and migration after injury



Myoepithelial Cells of Submucosal Glands Can Function as Reserve Stem Cells to Regenerate Airways after Injury

Aleksandra Tata,¹ Yoshihiko Kobayashi,¹ Ryan D. Chow,² Jasmine Tran,¹ Avani Desai,¹ Abdull J. Massri,¹ Timothy J. McCord,³ Michael Dee Gunn,³ and Purushothama Rao Tata,^{1,4,5,6,*}

¹Department of Cell Biology, Duke University School of Medicine, Durham, NC 27710, USA

²Department of Genetics, Systems Biology Institute, Medical Scientist Training Program, Yale University School of Medicine, New Haven, CT 06520, USA

³Department of Medicine, Division of Cardiology, Duke University School of Medicine, Durham, NC 27710, USA

⁴Duke Cancer Institute, Duke University School of Medicine, Durham, NC 27710, USA

⁵Regeneration Next, Duke University, Durham, NC 27710, USA

⁶Lead Contact

*Correspondence: purushothamarao.tata@duke.edu

<https://doi.org/10.1016/j.stem.2018.03.018>

SUMMARY

Cells demonstrate plasticity following injury, but the extent of this phenomenon and the cellular mechanisms involved remain underexplored. Using single-cell RNA sequencing (scRNA-seq) and lineage tracing, we uncover that myoepithelial cells (MECs) of the submucosal glands (SMGs) proliferate and migrate to repopulate the airway surface epithelium (SE) in multiple injury models. Specifically, SMG-derived cells display multipotency and contribute to basal and luminal cell types of the SMGs and SE. *Ex vivo* expanded MECs have the potential to repopulate and differentiate into SE cells when grafted onto denuded airway scaffolds. Significantly, we find that SMG-like cells appear on the SE of both extra- and intra-lobular airways of large animal lungs following severe injury. We find that the transcription factor SOX9 is necessary for MEC plasticity in airway regeneration. Because SMGs are abundant and present deep within airways, they may serve as a reserve cell source for enhancing human airway regeneration.

INTRODUCTION

Tissue homeostasis is fueled by resident stem/progenitor cells or by self-duplication of differentiated cells (Hogan et al., 2014; Visvader and Clevers, 2016). In adult tissues, stem/progenitor cells are located in specialized microenvironments tailored to accommodate the tissue needs (Hsu et al., 2011; Pardo-Saganta et al., 2015a; Scadden, 2014). In most tissues, stem cells and committed mature cells are thought to be irreversible and lineage restricted under homeostatic conditions, but recent studies indicate that cells can be experimentally coaxed to exhibit plasticity (Donati et al., 2017; van Es et al., 2012; Rompolas et al., 2013;

Stange et al., 2013; Tata and Rajagopal, 2016; Tata et al., 2013; Van Keymeulen et al., 2011). Specifically, in severe injury, committed cells revert to a stem cell state or cells from one region can migrate and display characteristics of an adjacent tissue to quickly replace damaged cells (Blanpain and Fuchs, 2014; Tetteh et al., 2015). For example, lineage tracing studies in skin epidermis revealed that cells from hair follicles and sebaceous glands can migrate and regenerate interfollicular epidermis following injury (Donati et al., 2017; Rompolas et al., 2013). In the small intestine, LGR5⁺ cells serve as stem cells and normally self-renew and generate all cell types of the villi (Barker et al., 2007). However, recent studies found that cells at the +4 position in the crypt, marked by Bmi1⁺/Tert⁺/HopX⁺, have the ability to generate LGR5⁺ cells following severe injury to crypts. Such cells have been proposed to serve as “reserve” stem cells for their ability to generate tissue-specific resident stem cells after injury. Taken together, these and other results suggest that tissues harbor reserve or facultative stem cells that can act when resident stem cells are lost (Tetteh et al., 2015). Such plasticity mechanisms offer therapeutic avenues for enhancing regeneration, particularly following severe injuries that damage resident stem cells. However, the cellular sources and the mechanisms associated with such plasticity are poorly understood (Blanpain and Fuchs, 2014; Merrell and Stanger, 2016; Rajagopal and Stanger, 2016; Tata and Rajagopal, 2017).

Epithelial tissues, such as the airway luminal surface epithelium (SE), require a rapid response to injury to prevent secondary damage and loss of barrier function (Hogan et al., 2014; Kotton and Morrisey, 2014). Airway epithelium consists of two broad tissue domains: the pseudostratified SE and submucosal glands (SMGs). In the SE, lineage tracing analysis has identified multiple region-specific stem/progenitor cells along the proximo-distal axis of the airway. In the mouse trachea and human extra and intra-lobar airways, the epithelium consists of 3 major cell types: basal stem cells and columnar luminal secretory and multiciliated cells. The basal cells self-renew and generate secretory club cells and multiciliated cells in homeostasis and regeneration (Borthwick et al., 2001; Cole et al., 2010; Franks et al., 2008; Ghosh et al., 2011; Hogan et al., 2014; Hong et al., 2004a,



2004b; Liu et al., 1994; Pardo-Saganta et al., 2015b; Rock et al., 2009). In the SMGs, the epithelial populations consist of distal acini and the proximal collecting ducts that connect them to the SE. Collecting ducts are morphologically similar to the SE and consist of basal and luminal cells whereas the distal SMGs contain luminal serous and mucous cells and basally located contractile myoepithelial cells (MECs) (Crystal et al., 2008; Franks et al., 2008; Hegab et al., 2010, 2011, 2012; Liu and Engelhardt, 2008; Wansleeben et al., 2014). In the human, SMGs are present throughout the cartilaginous airways. In mice, SMGs are primarily located in the proximal part of the trachea spanning the submucosal region between the larynx and cartilage-1 but are occasionally found up to cartilage-3, depending on the mouse strain, size, and age (Borthwick et al., 1999; Liu and Engelhardt, 2008).

At homeostasis, both SE and SMG cells are highly quiescent and display low turnover rates. Following injury, SE basal stem cells and SMG cells quickly respond to proliferate and generate both basal and luminal cells in the respective tissue domains. Intriguingly, a recent cell lineage tracing study, using a *Krt14-crePR* driver line, has suggested that SMG duct cells contribute to SE following hypoxia-induced airway injury (Hegab et al., 2011). However, KRT14 is also expressed in a subset of SE basal cells. Therefore, additional studies using a lineage-tracing approach that is specific to SMG cells are required to definitively establish whether SMG cells can generate SE cells. Furthermore, unique markers that distinguish SMG epithelial cells from SE cells are needed to establish whether the cells from these two compartments interconvert and exhibit plasticity in homeostasis and after injury.

Here, using single-cell RNA sequencing followed by stringent lineage tracing and functional assays, we demonstrate that MECs of the SMGs act as reserve stem cells that can proliferate, migrate, and repopulate both basal and luminal compartments of the SE and SMGs following multiple injuries, including toxic gas exposure or viral infection. We find that SMG-derived MECs and their progeny lose the characteristics of SMGs and display features of SE cells. Using large-animal injury models, we demonstrate that SMG-like cells emerge in pig extra-lobular as well as intra-lobular airway SE following severe injury. Using SOX9 loss-of-function mouse models, we also demonstrate that this transcription factor (TF) is necessary for MEC proliferation and migration to the SE after injury. Such conservation in cellular plasticity between small- and large-animal models suggests that SMGs embedded deep within the human airway submucosa likewise harbor a reserve stem cell population that can significantly contribute to repair and regeneration.

RESULTS

Single-Cell RNA-Seq Identifies Cells Expressing SMG Markers in SE following Naphthalene-Induced Injury

Recent studies using lineage tracing analysis coupled with injury repair models have identified distinct region-specific cell populations that participate in airway regeneration (Hogan et al., 2014; Tata and Rajagopal, 2017). However, the cellular identities and cell states associated with regenerating tissues are poorly understood. To study airway injury repair processes, we performed RNA sequencing (RNA-seq) analysis on single cells isolated

following naphthalene-induced injury. Naphthalene (naph) has been widely used to study airway injury repair mechanisms. Whereas it is generally considered that secretory cells are the primary target of naphthalene, it has been noted that ciliated cells are also lost to some extent in this injury model (Buckpitt et al., 1995; Cole et al., 2010; Stripp et al., 1995; Van Winkle et al., 1995). Under our experimental conditions, most of the luminal SE cells, not just club cells, were lost within 24 hr in the naphthalene-treated airways, but not in oil-treated controls. Overall, about $76\% \pm 1.74\%$ (mean \pm SEM; $n = 3$) of the total (DAPI $^+$) cells were lost in the tracheal SE on day 1 post-injury (Figures S1A and S1B). Immunohistochemistry (IHC) for KRT5 and KRT8, markers of basal and luminal cells, respectively, revealed both of these cell types were lost, leaving behind small patches of basal cells (Figure S1C). Our attempts to isolate and recover a significant number of viable SE cells prior to day 5 for single-cell RNA-seq (scRNA-seq) analysis were unsuccessful. We therefore chose day-5 trachea to enzymatically dissociate and collect SE cells from naphthalene-treated animals for scRNA-seq analysis. Quantification of total cell number and expression of basal (KRT5) and luminal (KRT8) cell markers indicated that most of the SE cells were recovered by day 5 (Figure S1). To avoid any artifacts in gene expression signatures, we proceeded to Drop sequencing (Drop-seq)-based scRNA-seq without performing fluorescence-activated cell sorting (FACS) (Figure 1A).

After excluding non-epithelial cells, the final scRNA-seq dataset was comprised of 139 cells. Across all the single cells analyzed, an average of $22,149 \pm 1,019$ (mean \pm SEM) unique reads mapped to the mouse transcriptome. $1,489 \pm 30.73$ (mean \pm SEM) unique genes were found to be expressed (\log_2 reads per million mapped, rpm ≥ 1) in individual cells. We performed k-means clustering and visualized the data by t-distributed stochastic neighbor embedding (t-SNE) to reveal potential underlying structure in the data (van der Maaten, 2014). Five distinct clusters were identified across the 139 single cells (Figure 1B). Differential expression analysis revealed the key genes associated with each of the 5 clusters (Figure 1C). Clusters 1, 2, and 3 were determined to be different subtypes of luminal cells on the basis of high *Krt8* expression, a universal marker of luminal epithelial cells in diverse columnar epithelial tissues (Figure 1E). Of the three luminal subtypes, Lum-1 most closely resembled normal airway secretory cells, as these cells were marked by *Scgb1a1*, *Lyz*, and *Scgb3a2* expression (Figure 1F). These cells also highly expressed cytochrome p450 genes, including *Cyp4a12b* and *Cyp2a5*, further indicating that these are secretory cells of the airways. Lum-2 cells were characterized by expression of inflammation-related genes *Ifit1b1* and *Irf7*. On the other hand, Lum-3 cells were not only defined by *Ppp1r1b*, *Bspry*, and *Lcn2* expression but also expressed *Ltf* (Figure 1G), which encodes the lactoferrin protein characteristic of serous cells of the mouse SMGs (Figure 1G). Interestingly, 5/41 (12.2%) of Lum-3 cells expressed *Sox9*, which encodes a transcription factor known to be highly and specifically expressed in developing SMGs (Figure 1H) and other glandular tissues (Anderson et al., 2017). Based on their distinct expression profiles, Lum-3 cells do not appear to correspond to a luminal cell type that is normally present in the uninjured airway epithelium.

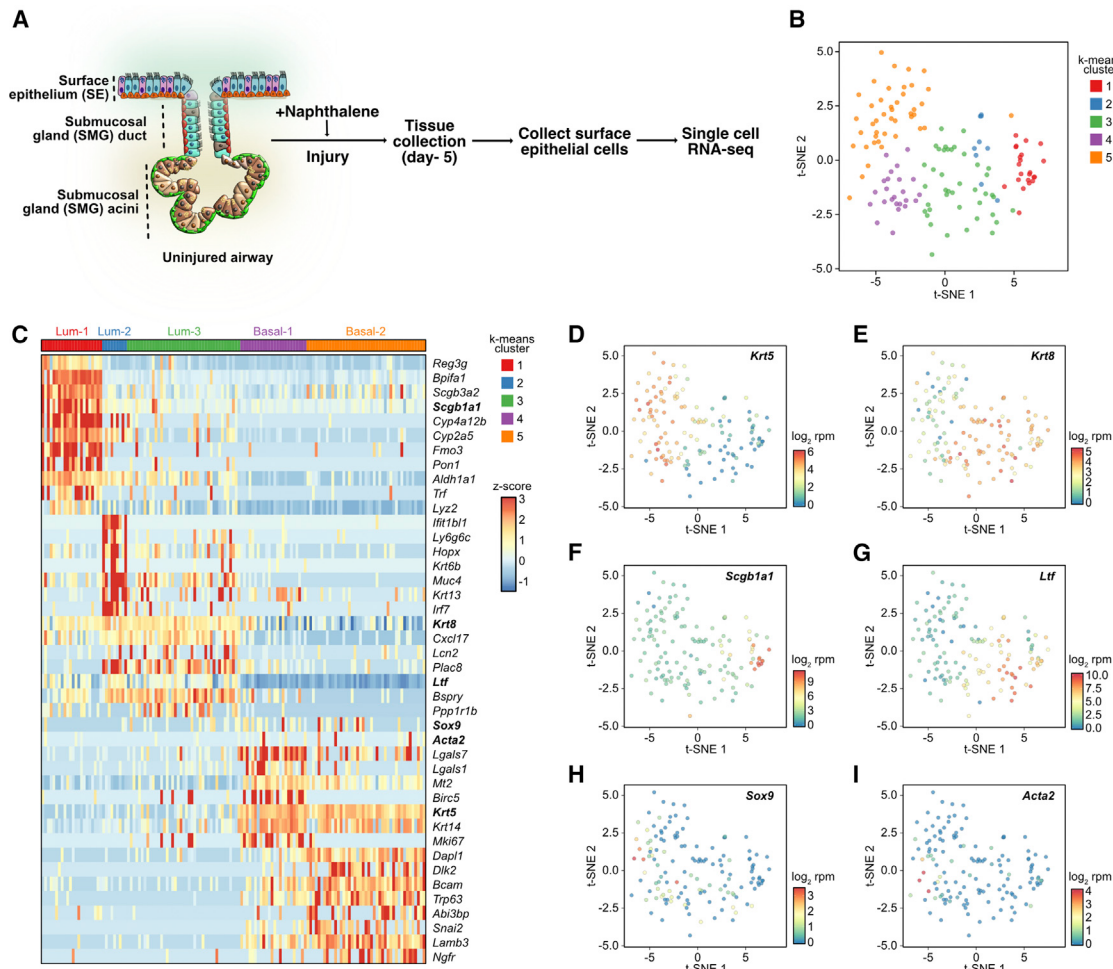


Figure 1. Single-Cell RNA-Seq Reveals a Population of Gland-like Cells in the Airway SE following Naphthalene Injury

(A) Schematic of experimental design and single-cell library preparation.

(B) t-SNE visualization of the single-airway epithelial cells after naphthalene injury (n = 139 cells). Cells are color coded by k-means clusters.

(C) Heatmap of genes associated with the 5 clusters (Lum-1, Lum-2, Lum-3, basal-1, and basal-2). Values are shown in terms of Z scores. Gene names in bold are individually featured in subsequent panels.

(D–I) t-SNE visualization of single-airway epithelial cells after naphthalene injury (n = 139 cells). Cells are color coded by normalized expression of the indicated genes: (D) Krt5; (E) Krt8; (F) Scgb1a1; (G) Ltf (lactoferrin); (H) Sox9; and (I) Acta2.

See also Figure S1.

Clusters 4 and 5 expressed high levels of basal cell markers, including *Krt5*, *Krt14*, and *Trp63* (also known as *Tp63*; Figure 1D) and were therefore termed basal-1 and basal-2. Basal-1 expressed high levels of *Lgals7*, *Lgals1*, *Birc5*, as well as *Mki67*, which is a marker of proliferation. In contrast, basal-2 was defined by *Sna1i*, *Lamb3*, *Ngfr*, *Dlk2*, and *Dap1*. Intriguingly, a fraction of the total basal cell population expressed *Sox9* (17/67 cells or 25.4%; Figure 1H) and *Acta2* (also known as alpha-smooth muscle actin; 7/67 cells or 10.4%; Figure 1I). Of note, *SOX9* and *ACTA2* protein are not normally expressed in the SE but are known to be expressed in developing SMGs (*SOX9*) or in myoepithelial cells of the SMGs (*ACTA2*). Collectively, scRNA-seq revealed the presence of subpopulations of cells expressing canonical SMG markers in both the luminal and basal compartments of the airway SE 5 days following naphthalene-induced injury.

Airway Luminal SE Harbors Cells Expressing SMG Cell Markers following Naphthalene-Induced Injury

To validate the scRNA-seq findings, we administered naphthalene or corn oil to mice and collected trachea on days 1, 3, and 5 for whole-mount and section IHC. In controls, KRT5 expression was observed in basal cells of the SE and SMGs, whereas ACTA2 was clearly confined to SMG myoepithelial cells (Figures 2A and 2B). Notably, SOX9 was expressed in both luminal and basal layers of the SMG cells, but not in the SE, indicating that SOX9 serves a unique pan-SMG marker distinguishing SMGs from SE cells. In naphthalene-treated airways, significant changes were seen following injury. In particular, we observed stellate-shaped cells co-expressing ACTA2, TP63, and KRT14, markers characteristic of myoepithelial cells of the SMGs, in regions around the gland pits where SMG ducts are connected to the SE (Figures 2A and S1D). Significantly, we also observed

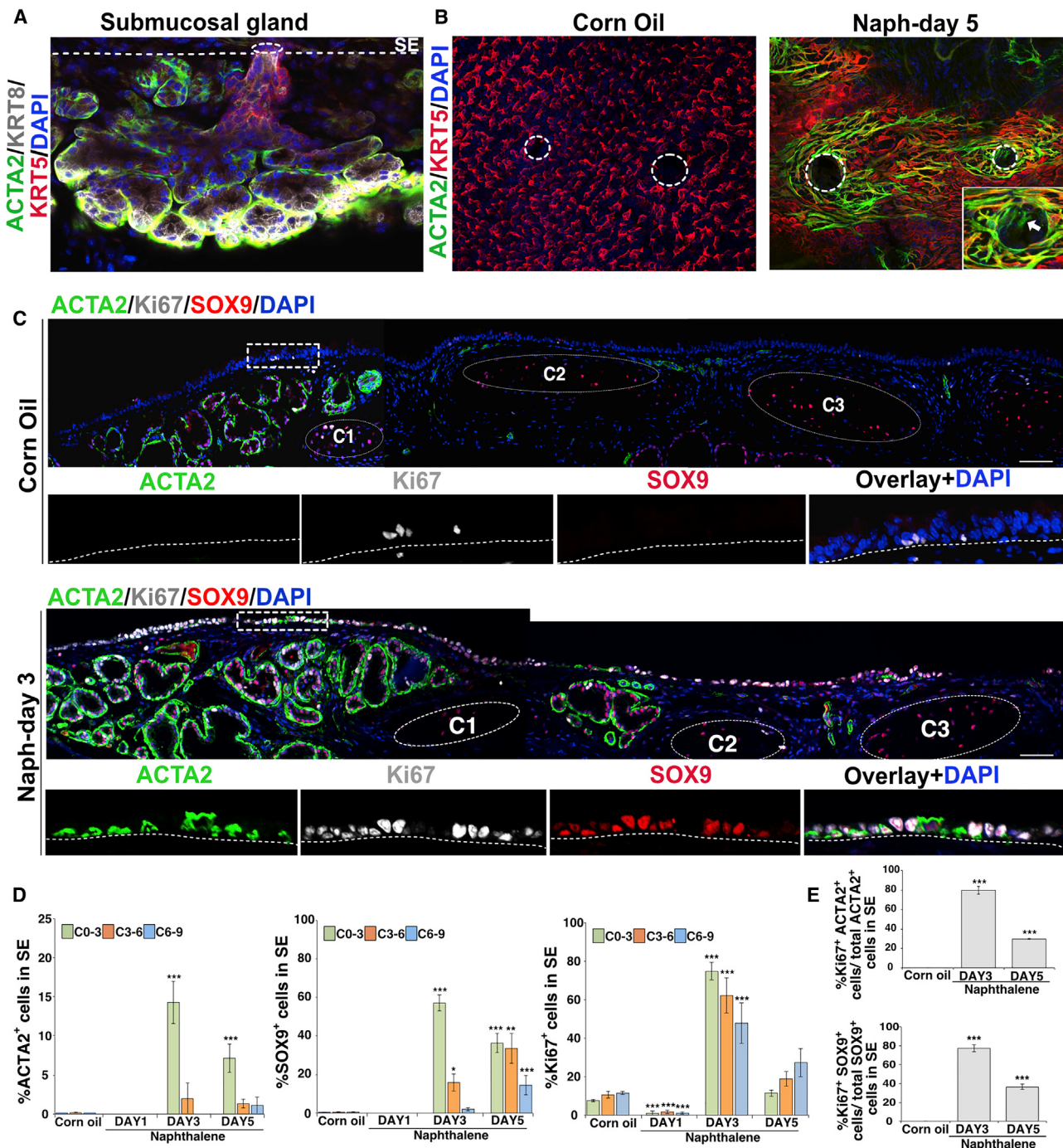


Figure 2. Airway Luminal SE Harbors Cells Expressing SMG Cell Markers following Naphthalene-Induced Injury

(A) Whole-mount IHC of SMG for myoepithelial cell marker ACTA2 (green), basal cell marker KRT5 (red), luminal cell marker KRT8 (gray), and nuclear DAPI (blue). The dotted line indicates border between SMG and SE. The scale bar represents 50 μ m.

(B) Whole-mount IHC staining of tracheal SE in corn oil or naphthalene (naph)-treated mice at day 5 after injury. ACTA2 (green), KRT5 (red), and DAPI (blue) are shown. Dotted circles indicate gland pore opening. Higher magnification image of the gland pore is shown in inset right bottom. The scale bars represent 50 μ m; n = 3.

(C) (Large panels) Tracheal sections from naphthalene exposed (day 3) or control (corn oil) mice stained for ACTA2 (green), SOX9 (red), and Ki67 proliferation marker (gray). Large panels were generated by aligning and stitching individual images. (Small panels) Single markers are shown for regions delineated by dotted box. Dotted circles indicate cartilage rings marked as C1-C3. The scale bar represents 50 μ m.

(legend continued on next page)

SOX9 in SE cells of the naphthalene-administered airways, but not in corn-oil-treated controls. To temporally map these changes, we performed IHC analysis for ACTA2 in combination with SOX9 and Ki67, a marker of proliferating cells, at different times following injury. We then counted the ACTA2⁺, SOX9⁺, and Ki67-expressing cells on the SE on days 1, 3, and 5 in different regions along the proximo-distal axis. On day 3 post-injury, most of the markers are found between cartilage 0 and 3 (14.1% \pm 2.74% ACTA2⁺ cells in naph [n = 3] versus 0.06% \pm 0.06% ACTA2⁺ cells in controls [n = 3]; 57.08% \pm 4.07% SOX9⁺ cells in naph [n = 4] versus 0.19% \pm 0.12% SOX9⁺ cells in controls [n = 3]; 74.77% \pm 4.49% Ki67⁺ cells in naph [n = 4] versus 7.53% \pm 0.63% Ki67⁺ cells in controls [n = 3]; mean \pm SEM). At later times, the distribution of ACTA2⁺ and SOX9⁺ cells extended to cartilage 3–6 and 6–9, suggesting that the SMG-like cells migrate from proximal to distal regions of the airways. Interestingly, a sizeable number of the ACTA2⁺ (76.87% \pm 3.94%) and SOX9⁺ (77.32% \pm 3.69%) cells also expressed Ki67, indicating that SMG-like cells on the SE are highly proliferative (Figure 2E). Consistent with previous studies, naphthalene also caused significant damage to the SMG tissue, as shown by loss of mucous and serous cells (Liu and Engelhardt, 2008; Figure S1D). Interestingly, on day 1, we noticed more proliferating cells in SMGs than in SE (Figure S1D). Taken together, our data suggest that cells expressing SMG cell markers first appear on the SE following naphthalene-induced airway injury and that these cells are highly proliferative and migratory.

SMG-like Cells Appear on SE in Multiple Injury Models

Different classes of injury models, such as sulfur dioxide (SO₂) and chlorine inhalation, influenza infection, and hypoxia, have been used to study repair mechanisms in trachea, where SE basal stem cells were thought to serve as progenitor cells to replenish lost epithelium (Rock et al., 2011; Tata et al., 2013). To test whether the plasticity mechanisms observed in naphthalene-induced injury model occur in other injury models, we subjected wild-type C57BL/6 mice to SO₂ or mouse-adapted H1N1 (PR8) infection-induced injury, both known to cause severe damage to luminal cells of the SE within 48 hr post-exposure, leaving behind few KRT5⁺ basal cells (Figure S2A). We collected tissues on day 5 post-injury and performed IHC for SOX9 and ACTA2 (Figure S2) and found that SMG-like cells appeared in SE of SO₂ and PR8 virus administered mice. However, fewer SOX9⁺ ACTA2⁺ cells were observed in SE of SO₂ and PR8 virus administered airways compared to naphthalene-injured SE. Of note, we observed a significant difference in the degree of injury in SO₂ and PR8 virus administered airway SE compared to naphthalene injury models (Figures S2B and S2C). To determine whether a correlation exists between the number of SMG-like cells and degree of injury, we performed a similar quantification analysis as for naphthalene injury. We observed significantly fewer SMG cell markers on airway SE on

day 3 post-SO₂ (1.19% \pm 0.62% SOX9⁺ cells and 0.09% \pm 0.09% ACTA2⁺ cells; n = 3) or PR8-induced (3.05% \pm 1.12% SOX9⁺ and 1.31% \pm 0.80% ACTA2⁺ cells; n = 3) injury compared to naph injury (57.08% \pm 4.07% SOX9⁺ and 14.1% \pm 2.74% ACTA2⁺ cells; n = 3; mean \pm SEM; Figures 2D and S2D–S2I). These data suggest that the degree of damage influences the extent of cell plasticity in different injury models (O'Koren et al., 2013). Nevertheless, a significant number of ACTA2⁺ (37.36% \pm 8.96% in SO₂ and 42.33% \pm 5.76% in PR8 infection) and SOX9⁺ (44.17% \pm 10.44% in SO₂ and 47.54% \pm 5.20% in PR8 infection) cells co-expressed Ki67, indicating that the SMG-like cells that emerge onto the SE are again highly proliferative (Figures S2F and S2I). Taken together, our data suggest that SMG-derived cells contribute to SE in multiple injury models.

SMG-Derived Sox9-Lineage-Labeled Cells Repair SE and Contribute to Both Luminal and Basal Cells following Injury

To test the hypothesis that cells of the SMG contribute to SE repair, we bred a mouse line, *Sox9-creER;R26-LSL-tdTomato* (hereafter referred to as *Sox9-tdt*), in which tamoxifen administration specifically and permanently induces the expression of a red fluorescent protein, *tdTomato* (*tdt*), in *Sox9*-expressing cells with 93% efficiency. We observed efficient labeling of both basal and luminal cells of the SMG ducts and acini, but not the SE (Figures 3A, 3B, and S3A). Of note, *Sox9-tdt* lineage-labeled cells do not contribute to SE even after a 10-month chase, indicating that SMGs do not normally contribute to SE lineages at homeostasis (Figure S3B). Thus, the *Sox9-tdt* model faithfully marks SMG cells and allows us to follow the fate of these cells following injury.

To prevent any residual tamoxifen from acting in response to injury, we administered tamoxifen at least 4–6 weeks prior to naphthalene-induced injury and tissues were collected on days 5, 10, and 20 post-injury for lineage tracing analysis. We identified large patches of lineage-labeled *Sox9-tdt* cells in the SE in injured airways, but not in control animals (Figure 3B). Quantification of *tdt*⁺ cells in the SE showed 67.7% of the total SE cells were derived from *Sox9-tdt* lineage-labeled SMG cells by day 20 following injury. We found that the lineage-labeled cells extend more distally over time (up to cartilage-4 on day 5 and cartilage-9 on day 20) on SE, consistent with *Sox9-tdt* cells being a migratory population (Figure 3B). Interestingly, lineage-labeled SMG-derived *tdt*⁺ cells express markers of basal (KRT5) and luminal cells (KRT8) and contribute to acetylated-tubulin-expressing (Ac-Tub⁺) ciliated cells and SSEA1⁺ secretory cells (Figures 3B–3D and S3C). However, we did not find SCGB1A1-expressing *Sox9-tdt* cells on day 20 post-naphthalene injury. To test whether club cells require longer to express other markers (SCGB1A1, SCGB3A2, and BPIFA1 [also known as PLUNC]), we isolated airways from *Sox9-tdt* mice on day 80 post-naphthalene injury. Marker analysis revealed *Sox9-tdt* cells expressing mature club cell markers (Figure 3D) on day 80 SE.

(D) Quantification of ACTA2⁺, SOX9⁺, and Ki67⁺ cells among total DAPI⁺ cells in SE in control and naph-injured mice. Data are shown as mean \pm SEM (n \geq 3 mice); *p \leq 0.05; **p \leq 0.01; ***p \leq 0.001). C0–3, C3–6, and C6–9 refer to SE spanning cartilage rings between 0–3, cartilage 3–6, and cartilage 6–9, respectively.

(E) Quantification of ACTA2⁺, SOX9⁺ co-expressing Ki67⁺ cells in SE of control and day 3 and day 5 post-naph injury. Data are shown as mean \pm SEM (n = 3; ***p \leq 0.001). p values were determined compared to controls.

See also Figures S1 and S2.

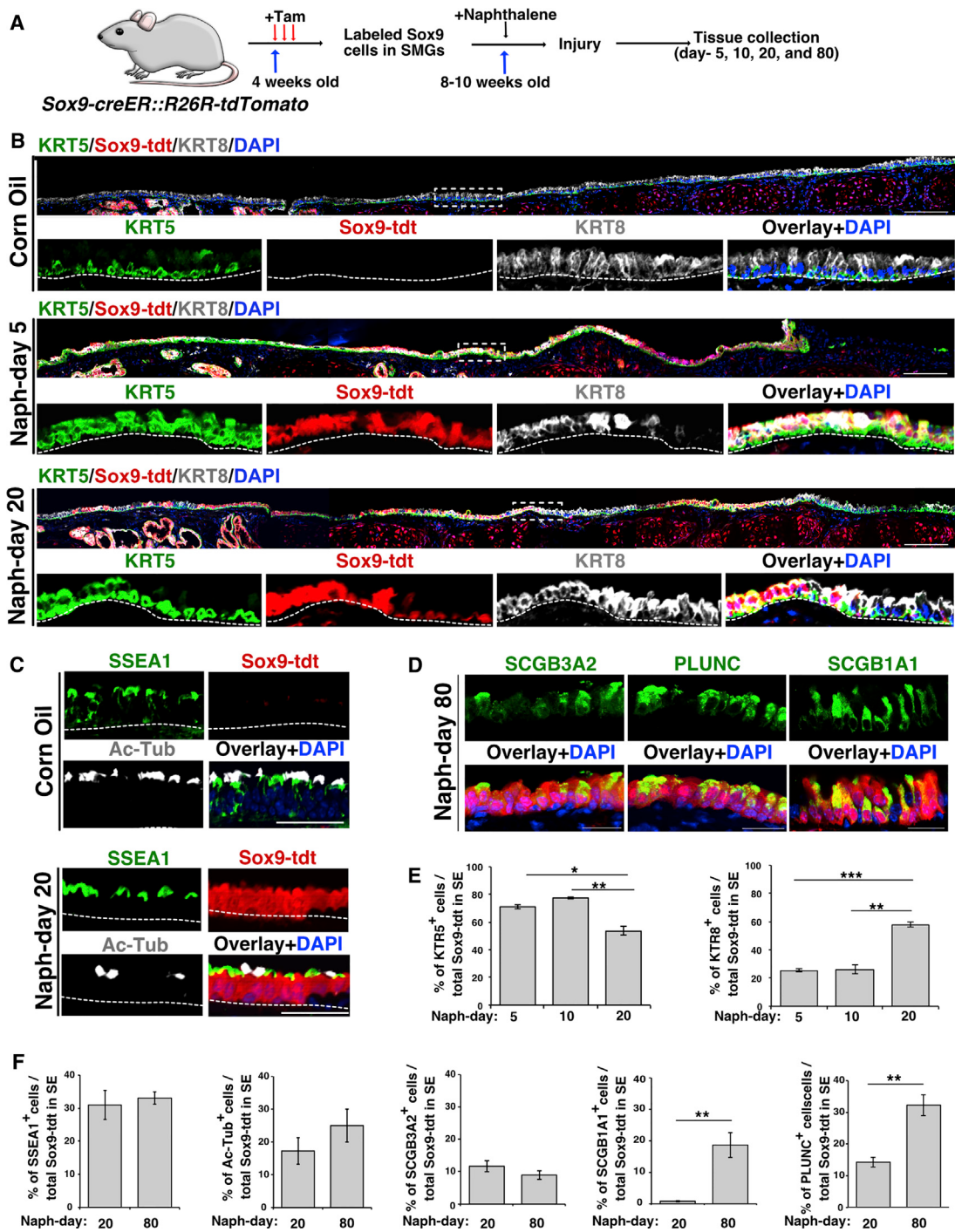


Figure 3. SMG-Derived Sox9-Lineage-Labeled Cells Repair SE and Contribute to Both Luminal and Basal Cells following Injury

(A) Schematic of Sox9-tdt lineage trace, naphthalene injury, and tissue collection.

(B) Co-staining of KRT5 (green) and KRT8 (gray) on tracheal sections collected from control and injured mice (days 5 and 20). The scale bar represents 50 μ m. Large panels were generated by aligning and stitching single pictures. Dotted box indicates region shown at high magnification in panels below. The dotted line separates SE and mesenchyme.

(C) Tracheal sections from Sox9-tdt naphthalene-injured (day 20) or control mice stained for SSEA1—secretory cell marker (green), AcTub (acetylated tubulin)—ciliated cell marker. Sox9-tdt (red) indicates Sox9-lineage-labeled cells; nuclear DAPI (blue). The scale bar represents 50 μ m.

(D) Staining of secretory cell markers: PLUNC; SCGB1A1; and SCGB3A2 (green) on day 80 naphthalene-injured Sox9-tdt (red) mice. Nuclear DAPI (blue) is shown. The scale bar represents 20 μ m.

(legend continued on next page)

Significantly, the proportion of Sox9-tdt⁺ KRT5⁺-expressing cells gradually declines over time ($70.8\% \pm 1.5\%$ on day 5 versus $77.6\% \pm 0.8\%$ on day 10 versus $53.7\% \pm 3.4\%$ on day 20; mean \pm SEM), whereas the proportion of KRT8⁺ lineage-labeled cells increases ($25.5\% \pm 1.2\%$ on day 5 versus $25.9\% \pm 3.1\%$ on day 10 [n = 3] versus $57.8\% \pm 1.7\%$ on day 20 [n = 3]; mean \pm SEM; Figure 3E). We also observed a similar trend in the number of SCGB1A1 ($1.29\% \pm 0.23\%$ on day 20 [n = 3] versus $22.94\% \pm 3.95\%$ on day 80 [n = 3]), PLUNC ($14.28\% \pm 1.52\%$ on day 20 [n = 3] versus $32.29\% \pm 3.31\%$ on day 80 [n = 4]), and Ac-Tub ($17.26\% \pm 4.04\%$ on day 20 [n = 3] versus $25.01\% \pm 5.07\%$ on day 80 [n = 4]; mean \pm SEM) expressing Sox9-tdt cells on the airway SE (Figure 3F). A model emerges in which Sox9-lineage-labeled cells are initially KRT5⁺ in the SMGs and proliferate, migrate, differentiate, and mature into SE luminal cells following injury (Figure 3). One of the characteristic functions of airway SE is to establish a polarized barrier with distinct apical junctional complexes. We therefore performed IHC for apical and basolateral polarity proteins, such as ZO1 and CDH1 (E-cadherin). Confocal microscopy revealed SMG-derived Sox9-tdt lineage-traced cells expressing ZO1 with a pattern similar to that seen in controls. Consistent with recent reports, we observed apical localization of ZO1 in early stages of regeneration where the epithelium is still composed of a single cell layer of cuboidal cells (Gao et al., 2015). The barrier therefore appears to be maintained at all times analyzed (Figure S3D). Together, our data demonstrate that SMG-derived Sox9-lineage-labeled cells repair and contribute to SE basal and luminal cells and establish airway barrier following injury (Figures 3 and S3).

SMG-Derived Acta2-Lineage-Labeled MECs Repair the SE and Contribute to Both Basal and Luminal Cells following Injury

To test whether the Sox9-tdt cells that emerge from SMG onto the SE following naphthalene-induced injury are derived from ACTA2⁺ MECs, we bred *Acta2-creER; R26R-LSL-tdTomato* mice (*Acta2-tdt*). Following tamoxifen administration, we observed tdt expression in 75% of the ACTA2- and TP63-expressing cells of the acini of SMGs, but not in SE or in SMG ducts (Figures 4 and S4). We then performed lineage tracing in control and injured animals and harvesting trachea on days 5, 12, 20, and 60 post-injury for IHC (Figure 4). We observed large patches of tdt⁺ cells in SE of the naphthalene-injured airways, but not in controls (Figure 4B), and 42.6% of the total SE cells were derived from *Acta2-tdt* lineage-labeled SMG cells on day 20 post-injury. Moreover, the distribution of *Acta2-tdt* cells moved distally from day 5 to day 12 post-injury (Figure 4B; data not shown). Similar to Sox9-tdt lineage, the *Acta2-tdt* lineage contributed to both basal and luminal cells and progressed from the KRT5⁺ basal cell state ($78.2\% \pm 5.3\%$ on day 5 versus $63.9\% \pm 4.8\%$ on day 12 versus $53.48\% \pm 1.36\%$ on day 20; n = 3; mean \pm SEM) to the KRT8⁺ luminal state ($21.5\% \pm 5.4\%$ on day 5 versus $36.6\% \pm 2.2\%$ on day 12 versus $46.51\% \pm 1.36\%$ on day 20; n = 3; mean \pm

SEM; Figure 4D). In addition, *Acta2-tdt* cells also expressed acetylated tubulin and SSEA1, markers of ciliated and secretory cells, respectively, on day 20 post-injury (Figures 4C and 4D). Again, we observed SCGB1A1 expression in *Acta2-tdt*-derived SE cells only at late stages (Figure 4E). Taken together, our data demonstrate that ACTA2⁺ MECs contribute to repair and regenerate SE following injury (Figure 4).

SMG-Derived Acta2-Lineage-Labeled MECs Contribute to Both Basal and Luminal Cells of the SMGs Repair *In Vivo* following Injury

Distinct stem/progenitor cells are thought to contribute to distinct compartments in tissue homeostasis and regeneration in other epithelial tissues, such as mammary glands (Van Keymeulen et al., 2011). Currently, it is not known whether ACTA2⁺ basal MECs of the SMGs have the ability to contribute to luminal cells of the SMGs. To test this, we utilized our naphthalene-induced injury model, which causes significant damage to luminal cells of the SMGs. In control mice, we found no contribution of *Acta2-tdt*-lineage-labeled cells to luminal cells (Figure S4). By contrast, a significant number of luminal cells were derived from the *Acta2-tdt* lineage in naphthalene-treated airways ($18.99\% \pm 2.65\%$ KRT8⁺ *Acta2-tdt* cells in naph versus 0 KRT8⁺ *Acta2-tdt* cells in control mice; mean \pm SEM; n = 3; Figure S4). Further analysis indicated that MEC-derived tdt⁺ luminal cells co-expressed lactotransferrin (LTF) ($48.53\% \pm 7.41\%$) or MUC5B ($21.92\% \pm 6.53\%$; mean \pm SEM; n = 3), indicating that MEC-derived cells contribute to both serous and mucous cells, respectively (Figure S4E). Taken together, our data demonstrate that MECs contribute to basal and luminal cells of the SMGs and SEs of trachea (Figures 4 and S4).

SMG-Derived MECs Display SE Basal Cell Characteristics *Ex Vivo*

Our *in vivo* lineage tracing experiments indicate that MECs of the SMGs can proliferate, migrate, and generate SE cells following injury. During this transition, the number of ACTA2⁺ cells sharply declines from day 3 to day 5 while the total number of cells increases on the SE, indicating that MECs transition from an ACTA2⁺ to ACTA2⁻ state characteristic of the basal cells of the SE. To study this phenomenon, we isolated MECs from SMGs of *Acta2-tdt* mice and cultured them *ex vivo*. The isolated cells replicated and formed small colonies *in vitro* by day 5. IHC for markers of MECs and basal cells on day-3 and day-5 cultures revealed that *Acta2-tdt* cells lost the expression of ACTA2 by day 5 while continuing to express the basal cell markers, KRT5, TP63, and KRT14 (Figures 5A, 5B, and S5A). We also observed the expression of AQP3, NGFR, and ITGA6, other markers of basal cells at late times (Figure S5B). During this transition, MEC-derived *Acta2*-lineage-labeled cells changed their shape from a stellate to cobblestone morphology (Figures 5A and 5B). These data suggest that MECs can proliferate and change to SE basal-cell-like cells in *ex vivo* cultures.

(E) Quantification of KRT5⁺ and KRT8⁺ cells among total Sox9-tdt⁺ cells in SE on days 5, 10, and 20 post-naphthalene injury. Data are shown as mean \pm SEM (n = 3; *p ≤ 0.05 ; **p ≤ 0.01 ; ***p ≤ 0.001).

(F) Quantification of SSEA1⁺, Ac-Tub⁺, SCGB3A2⁺, SCGB1A1⁺, and PLUNC⁺ cells among total Sox9-tdt⁺ cells in SE on days 20 and 80 post-naphthalene injury. Data are shown as mean \pm SEM (day 20: n = 3; day 80: n = 4 for all markers except SCGB1A1 [n = 3]; *p ≤ 0.05 ; **p ≤ 0.01 ; ***p ≤ 0.001). See also Figure S3.

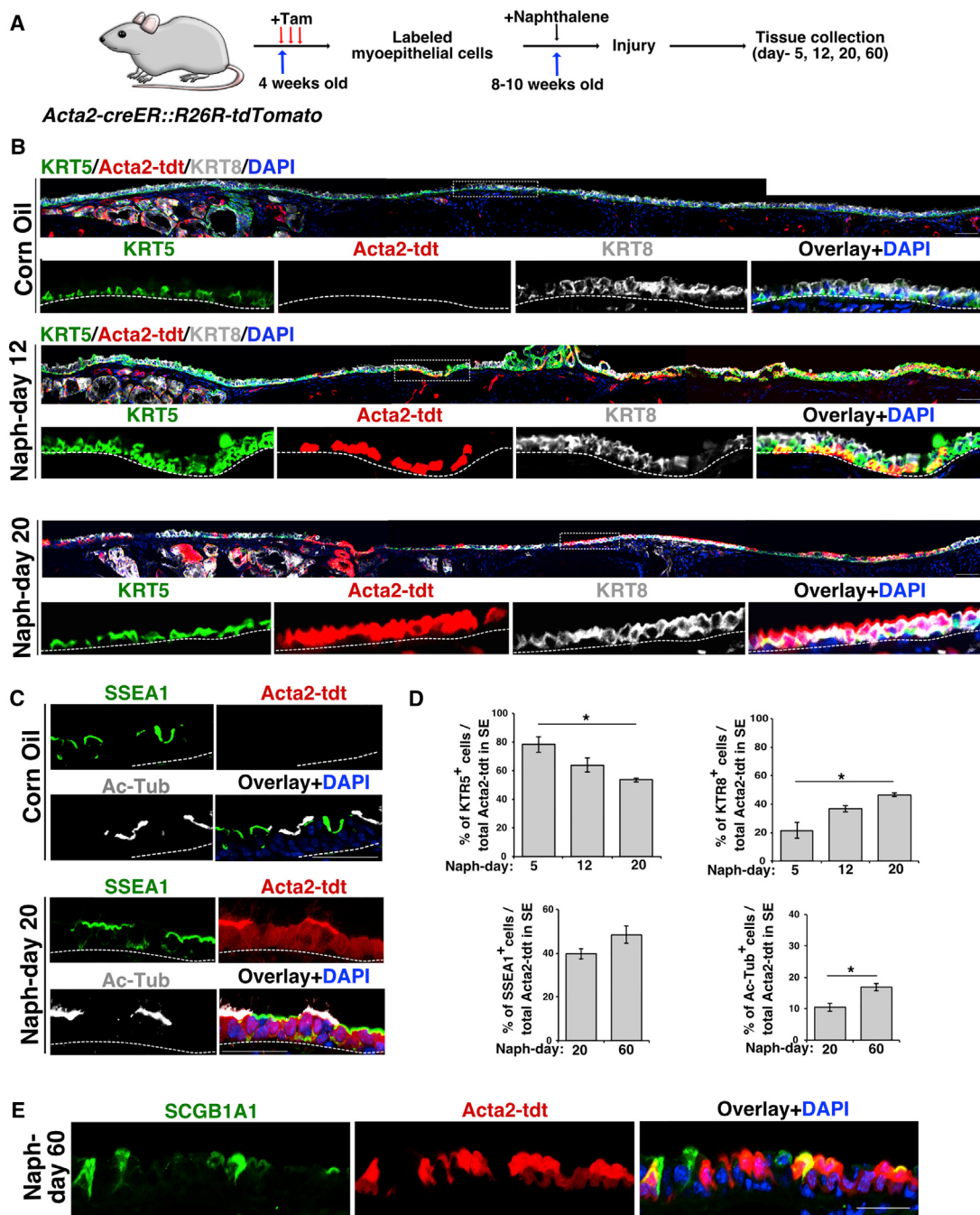


Figure 4. SMG-Derived Acta2-Lineage-Labeled MECs Repair the SE and Contribute to Both Basal and Luminal Cells following Injury

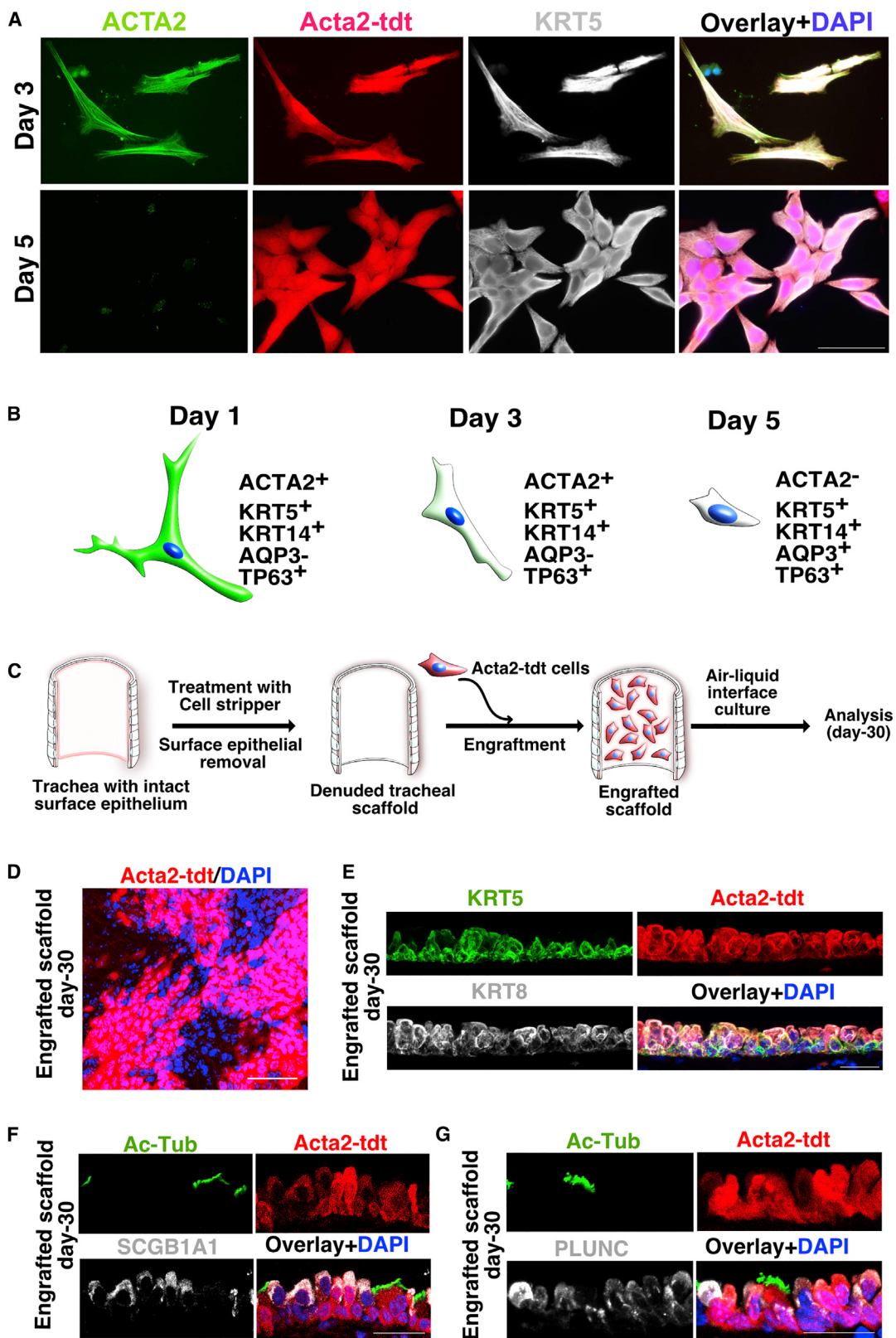
(A) Schematic of experimental design to label and trace Acta2-expressing myoepithelial cells in naphthalene-induced injury model.

(B) Tracheal sections from Acta2-tdt naphthalene-injured (days 12 and 20) or control mice stained with KRT5 (green) and KRT8 (gray). Acta2-tdt lineage-traced (red) and nuclear DAPI (blue) are shown. The scale bar represents 50 μ m. n = 3. Large panels were generated by aligning and stitching single pictures. Dashed line box indicates region of higher magnification shown in lower panel. The dashed line separates the SE and mesenchyme.

(C) Co-staining of SSEA1 (green) and Ac-Tub (gray) in naphthalene (day 20)-injured and control Acta2 lineage-traced (red) mice. DAPI was used to stain the nuclei (blue). The scale bar represents 50 μ m. The dashed line separates the SE and mesenchyme.

(D) Quantification of KRT5⁺, KRT8⁺ (naph days 5, 12, and 20), SSEA1⁺, and Ac-Tub⁺ (naph days 20 and 60) cells among total Acta2-tdt⁺ cells in SE in controls and naphthalene-injured mice. Data are shown as mean \pm SEM (n = 3; *p \leq 0.05; **p \leq 0.01; ***p \leq 0.001).

(E) IHC for SCGB1A1 (green) on Acta2-tdt (red) airways on day 60 post-naphthalene injury. Nuclear DAPI (blue) is shown. The scale bar represents 20 μ m. See also Figure S4.



(legend on next page)

MEC-Derived SE Basal-like Cells Proliferate, Engraft, and Generate Basal and Luminal Cell Types in *Ex Vivo* Engraftment Models

Our lineage tracing and *ex vivo* experiments suggest that MECs convert into SE basal-like cells. To test the potential of cultured MEC-derived basal cells, we utilized an *ex vivo* tracheal regeneration model. We generated tracheal scaffolds by removing the SE using a non-enzymatic method. Whole-mount IHC found that most of the SE basal and luminal cells were stripped away, leaving the denuded scaffold intact (Figure S5C). We then engrafted cultured Acta2-tdt MEC-derived basal-like cells onto the scaffolds and cultured them for 30 days in air-liquid-interface culture (Figure 5C). Whole-mount imaging revealed patches of lineage-labeled cells on the scaffold surface ($n = 7$ out of 12 scaffolds engrafted), suggesting that engrafted cells can proliferate and appropriately organize into epithelial sheets (Figure 5D). Subsequent section IHC showed that the engrafted cells generated both basal (KRT5 $^+$) and luminal (KRT8 $^+$) cells, including acetylated-tubulin-expressing ciliated cells as well as SCGB1A1- and PLUNC-expressing secretory cells (Figures 5E–5G). Thus, SMG-derived MECs have the ability to proliferate and generate SE cells *ex vivo* (Figures 5C–5G).

SMG-like Cells Appear in SE of Porcine Proximal and Distal Lobular Airway SE following Severe Injury

The distribution and abundance of SMGs varies between species. Unlike mouse airways, SMGs are present throughout cartilaginous airways in large mammals, including humans (Choi et al., 2000; Judge et al., 2014). Based on our current findings, we hypothesized that SMGs in large mammals have a greater ability to regenerate airway SE throughout the extra-lobular (i.e., trachea and bronchi) and intra-lobular airways (i.e., bronchioles). To test this hypothesis, we utilized a porcine airway injury model in which animals are exposed to chlorine gas at a concentration of 170 ± 8 ppm for 30 min to induce severe damage to the airways and alveoli (Gunnarsson et al., 1998; Wang et al., 2005). Filtered-air-exposed pigs served as controls (Figure 6A). We then isolated airway and lung tissues on day 2 post-injury for marker analysis. Histological analysis of large airways (trachea and bronchi) indicated that SE cells are sloughed off within 48 hr of chlorine exposure but remain intact in control animals (Figures 6 and S6A). Similar to the mouse naphthalene-induced injury model, SOX9 expression was observed in the SE of chlorine-exposed porcine airways, but not in controls where SOX9 is strictly confined to the SMGs (Figure 6B). Interestingly, the distribution

of SOX9 $^+$ cells in the SE of the bronchioles was not uniform but tightly correlated with regions that had severe damage (Figure 6B). Most of these SOX9 $^+$ cells also co-expressed Ki67, a marker for proliferating cells, indicating that SOX9 $^+$ cells are highly proliferative in these damaged tissues (Figure S6B). In many cases, patches of SOX9 $^+$ cells were seen in the SE extending from SMG acini and ducts. In contrast to mouse airway injury models, we did not find ACTA2 $^+$ cells on porcine SE after injury. To test whether porcine airway MECs have the ability to generate SE basal cells, we isolated, dissociated, and cultured SMGs from healthy porcine trachea similar to mouse MECs. We found small colonies of cells arising by day 3, and by day 5, 75% of the colonies were expressing MEC markers ACTA2 and KRT5 and proliferation marker Ki67. On day 9, KRT5 expression was maintained, but ACTA2 was no longer observed (Figure 6C). These data suggest that isolated porcine MECs have the ability to replicate and generate SE basal-like cells in *ex vivo* cultures. Our data suggest that SMG-derived cells act as reserve stem/progenitor cells throughout the airways in large animals and not just in the mouse trachea.

SOX9-Dependent Mechanisms Are Important for the Contribution of MECs to SE Repair after Naphthalene-Induced Injury

To understand the molecular mechanisms underlying the proliferation and migration of MECs in response to injury, we analyzed our scRNA-seq data for genes differentially expressed between homeostatic SMGs and SMG cells that appeared on the SE. We focused our analysis on MECs (EpCAM $^+$ Acta2 $^+$), as this population was one of the major contributors to SE repair. We obtained 25 EpCAM $^+$ Acta2 $^+$ SE cells from injured airways and 36 EpCAM $^+$ Acta2 $^+$ cells from homeostatic SMGs (Figure S7A). Further analysis identified 92 genes that were significantly different between these populations; gene ontology analysis identified genes involved in cell cycle, translation, cell migration, regulators of cytoskeleton, wound healing, inflammation, P53 signaling, Wnt signaling, and tumor necrosis factor (TNF)/nuclear factor κ B (NF- κ B) signaling (Figure S7B). Many of the differentially enriched genes were also known targets of transcription factors, including MYC, SOX9, FOXA1, TP63, SMAD4, and KLF4 (Figure S7B). Interestingly, many of the SOX9 targets were highly enriched for cell migration (*Fam60a*, *Ecm1*, *Iqgap1*, *Myh9*, *Itgb4*, *Tacstd2*, *Lgals3*, and *Anxa1*; Babbin et al., 2007; Noritake et al., 2005; Simionescu-Bankston et al., 2013; Vicente-Manzanares et al., 2009; Xiong et al., 2012; Zhu et al.,

Figure 5. MEC-Derived SE Basal-like Cells Proliferate, Engraft, and Generate Basal and Luminal Cell Types in *Ex Vivo* Engraftment Models

- (A) Myoepithelial cells of SMG display SE basal cell characteristics in culture. Cultured cells on days 3 and 5 co-stained with ACTA2 (green) and KRT5 (gray) are shown. Acta2-tdt (red) and nuclear DAPI (blue) are shown. The scale bar represents 50 μ m.
- (B) Schematic depicting the gradual loss of ACTA2 expression in SMG-derived MECs in culture.
- (C) Schematic representation of engraftment of cultured MECs on a denuded tracheal scaffold. Isolated, cultured myoepithelial cells were seeded on denuded trachea followed by air-liquid interface culture and analysis.
- (D) Whole-mount IHC analysis for tdt-expressing engrafted cells on tracheal scaffold. The scale bar represents 50 μ m.
- (E) Co-staining of KRT5 (green) and KRT8 (gray) on trachea engraftment sections. Acta2-tdt (red) and nuclear DAPI (blue) are shown. $n = 3$. The scale bar represents 20 μ m.
- (F) IHC for Ac-Tub (green) and SCGB1A1 (gray) on tissue sections from Acta2-tdt (red)-expressing cells engrafted on tracheal scaffold. Nuclear DAPI (blue) is shown. The scale bar represents 20 μ m.
- (G) Sections from engrafted scaffolds expressing Acta2-tdt (red) co-stained with Ac-Tub (green) and PLUNC (gray). Nuclear DAPI (blue) is shown. The scale bar represents 20 μ m.

See also Figure S5.

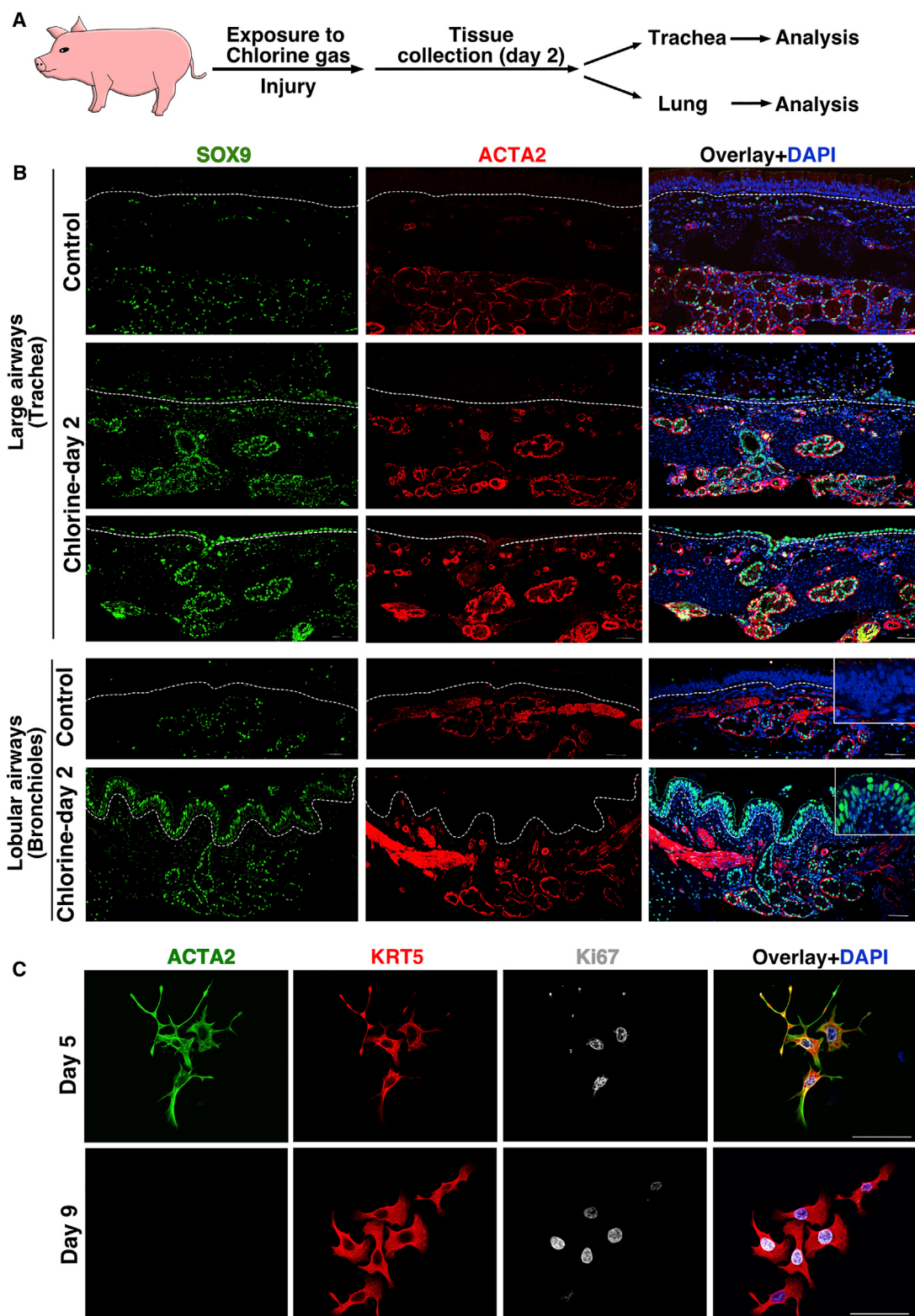


Figure 6. SMG-like Cells Appear in SE of Porcine Proximal and Distal Lobular Airway SE following Severe Injury

(A) Schematic representation of experimental design. Pigs were exposed to 170 ppm chlorine gas for 30 min followed by collection of trachea or lung tissue on day 2 post-injury.

(legend continued on next page)

2017; Figure 7A). Based on these data, we hypothesized that SOX9 plays an essential role in MECs proliferation and migration to the SE following injury. To test this hypothesis, we generated *Krt5-creER;Sox9^{fl/fl}* mice (*Krt5-SOX9-LOF*), which deletes Sox9 specifically in *Krt5*-expressing basal cell/myoepithelial cells upon tamoxifen administration (Figure 7B). We administered 3 doses of tamoxifen to *Krt5-SOX9-LOF* mice and control *Sox9^{fl/fl}* mice followed by naphthalene treatment. IHC for ACTA2 and SOX9 indicated loss of SOX9 specifically in MECs with $74.97\% \pm 3.34\%$ (mean \pm SEM; $n = 3$) deletion efficiency (Figure 7C) within SMG acini. On day 4 post-naphthalene injury, we observed significantly fewer DAPI⁺ cells on the SE compared to controls as well as significantly fewer SOX9- ($5.73\% \pm 4.78\%$ in *Krt5-SOX9-LOF* versus $32.49\% \pm 0.26\%$ in controls; $n = 3$), Ki67- ($34.28\% \pm 4.73\%$ in *Krt5-SOX9-LOF* versus $49.04\% \pm 2.33\%$ in controls; $n = 3$), and ACTA2 ($3.71\% \pm 3.05\%$ in *Krt5-SOX9-LOF* versus $11.74\% \pm 2.47\%$ in controls; $n = 3$; mean \pm SEM)-expressing cells on the SE, indicating that significantly fewer MECs proliferated and migrated to the SE after loss of Sox9 in MECs (Figures 7E and 7F). These data support a model in which SOX9 is essential for MECs proliferation and their migration to the airway SE after naph-induced injury, potentially through regulating a set of downstream target genes involved in this process.

DISCUSSION

Airway SMGs are highly abundant in human lungs, where they function as mucus-producing units, undergoing significant hypertrophy in conditions such as cystic fibrosis (CF), asthma, and chronic obstructive pulmonary disease (COPD) (Jeffery, 1991). Here, we demonstrate that MECs within the SMGs also serve as progenitors, migrating long distances to regenerate the SE following severe injury. Intriguingly, the plasticity we observed is proportional to the degree of injury and occurred in multiple forms of injury models (Figure S2). However, it is possible that many factors, including inflammation and other systemic factors, may also influence the degree of plasticity in different forms of injury models. Previous studies using *Krt14*-promoter-driven lineage tracing suggest that SMG duct cells contribute to SE repair following hypoxic injury. However, KRT14 is expressed in SE basal cells, making it difficult to determine the contribution of SMG duct cells to SE repair. scRNA-seq allowed us to identify SMG-like cells on SE following injury and revealed that SOX9 was specifically expressed in adult SMGs, but not in SE. Using myoepithelial-cell-specific lineage tracing models, we demonstrate that SMG-derived MECs contribute to the SE repair. Accounting for lineage labeling differences, 67.7% of SE cells were derived from *Sox9⁺* cells whereas 42.6% were derived from MECs. The different relative contribution of *Sox9*-tdt and *Acta2*-tdt cells suggests that cells other than MECs (*SOX9⁺ACTA2⁻*) within the SMGs also contribute to SE repair. Indeed, previous studies suggested SMG duct cells

contribute to SE repair (Hegab et al., 2012). Alternatively, SMG luminal cells may also contribute to the SE repair. Likewise, mammary gland MECs are shown to act as lineage-restricted mammary stem cells (Prater et al., 2014). Future studies are needed to uncover whether there are any subsets of MECs that possess higher “stemness,” as such subsets were recently demonstrated to play a major role in alveoli regeneration (Nabhan et al., 2018; Zacharias et al., 2018).

Our data support a model in which MECs migrate to the SE, lose their myoepithelial identity (defined by ACTA2 expression and morphology), and acquire SE basal cell characteristics following injury. The transition from MEC to airway basal cell may be driven by micro-environmental factors, such as the basement membrane or residual SE cells, or cell-autonomous mechanisms. Indeed, *Sox9*- and *Acta2*-lineage-derived cells did not express mature club cell marker (SCGB1A1) until several weeks after injury, indicating that some cell-autonomous mechanisms likely constrain the differentiation of SSEA1⁺ immature club cells into mature club cells.

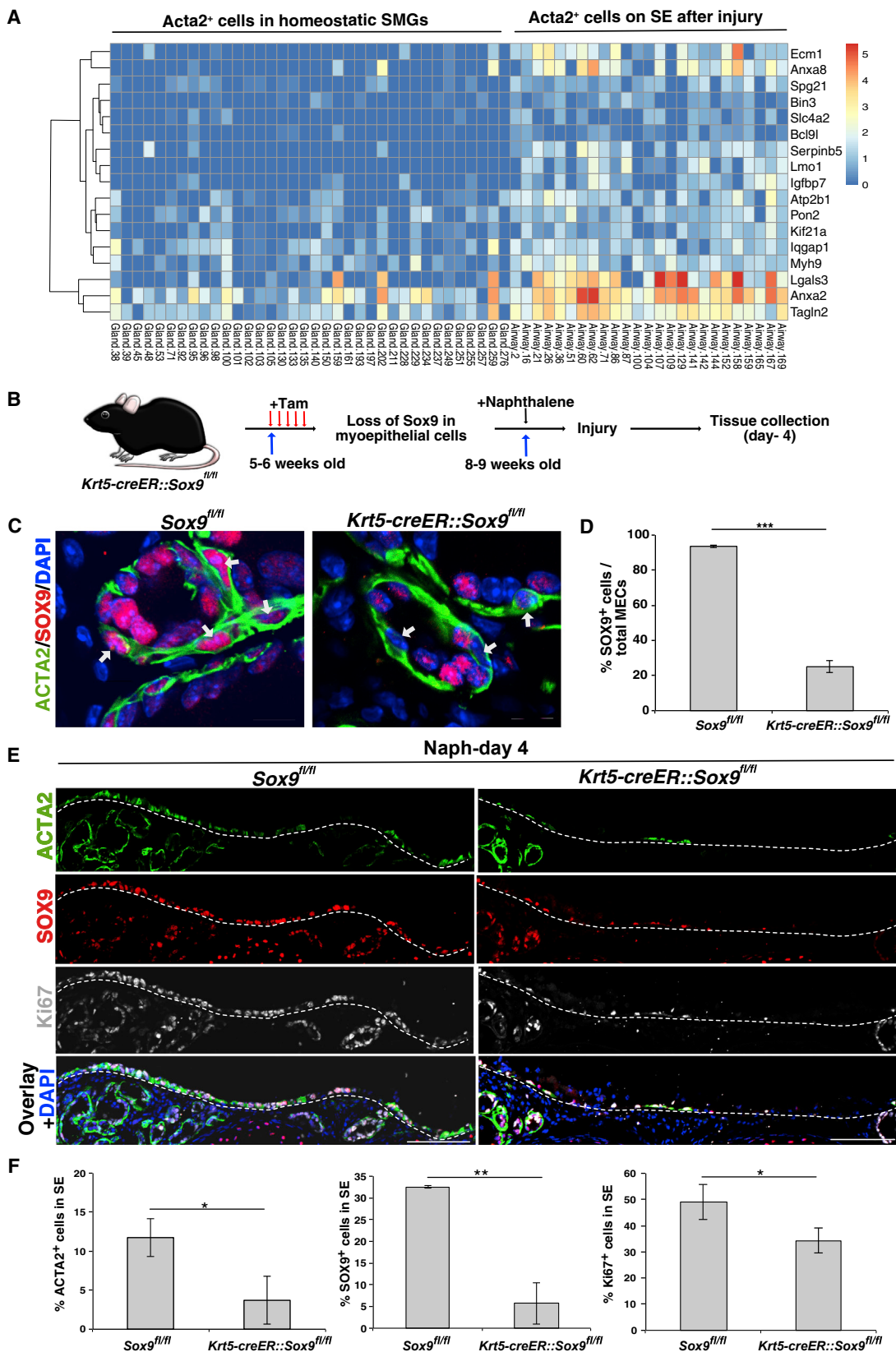
Recent studies have shown that MECs contribute to both basal and luminal lineages and act as multipotent progenitor cells during SMG development (Anderson et al., 2017). Interestingly, we find that MECs in the adult SMGs constrain their lineage potential at homeostasis but exhibit plasticity under adverse conditions. Such characteristics may thus qualify them to function as reserve multipotent stem cells (Blanpain and Fuchs, 2014; Merrell and Stanger, 2016; Tata and Rajagopal, 2016; Visvader and Clevers, 2016). Although this question remains an active area of investigation, it appears that, whereas lineage-restricted stem progenitor cells individually maintain the mammary basal and luminal compartments at homeostasis, a subpopulation either intrinsically possesses or acquires multipotency in transplantation assays or during pregnancy and lactation to contribute to all lineages (Rios et al., 2014; Van Keymeulen et al., 2011).

In contrast to SE, the lung SMGs are embedded deep within airway tissues, analogous to the intestinal crypts and gastric pits in the intestine and stomach, respectively. Such a location presumably protects the SMGs from normal wear and tear as well as airborne pathogens and toxic agents and enables them to serve as an important and overlooked source of reserve stem cells (Tetteh et al., 2015; Visvader and Clevers, 2016). Indeed, our large-animal model suggests that the SMG cells contribute significantly to both extra- and intra-pulmonary airway regeneration (Figure 6). SMGs are present throughout cartilaginous airways of the human lungs and likely play a critical role in endogenous regeneration after infection and injury. Although we observed many SOX9⁺ cells on the SE of porcine injured airways, these cells did not express ACTA2 like the mouse. SMGs are abundant in porcine airways, so perhaps duct cells alone are sufficient to repair SE. Alternatively, MECs may downregulate and eventually lose the expression of ACTA2 *en route* to SE. Indeed, our experiments in mice suggest

(B) Co-IHC for indicated markers on tracheal sections (upper panels) or lobular airways (lower panel) from control or chlorine-gas-exposed pigs. The dashed line separates the SE and mesenchyme. Inset in the upper panel shows the higher magnification images. The scale bar represents 50 μ m.

(C) MECs isolated from pig SMG display SE basal cell characteristics in culture. Cultured cells were fixed on day 5 or day 9 and co-stained with ACTA2 (green), KRT5 (red), Ki67 (gray), and nuclear DAPI (blue). The scale bar represents 50 μ m.

See also Figure S6.



(legend on next page)

that MECs quickly lose ACTA2 expression when they migrate to the SE or when placed in culture (Figures 4 and 5). Nevertheless, isolated porcine MECs displayed SE basal-like cell characteristics in cultures, suggesting that porcine MECs have the ability to generate SE basal cells (Figure 6).

Our scRNA-seq analysis not only identified SMG-like cells on the SE after injury but also revealed differentially expressed genes in ACTA2⁺ MECs in response to injury. Gene ontology analysis showed enrichment for different biological processes, including cell cycle and cell migration. Some genes were previously shown to be regulated by the transcription factor SOX9 in multiple tissues, including hair follicle stem cells (Adam et al., 2015). Although SOX9 was expressed in both homeostatic MECs and MECs following injury, it remains to be tested how and whether SOX9 regulates different downstream target genes in different cellular contexts. Indeed, it has been demonstrated that SOX9 binds on different target gene regulatory elements in different cellular contexts in hair follicles and is therefore recognized as a pioneer transcription factor (Adam et al., 2015).

Important questions for the future will be to determine whether Sox9⁺ SMG-derived SE persists in the airways, perhaps altering airway response to environmental agents, or whether SMG glands continue to replenish the SE following repeated injuries. This research motivates future work to elucidate how endogenous repair mechanisms can be enhanced therapeutically and provide important new insights into human respiratory health and disease.

STAR METHODS

Detailed methods are provided in the online version of this paper and include the following:

- KEY RESOURCES TABLE
- CONTACT FOR REAGENTS AND RESOURCE SHARING
- EXPERIMENTAL MODELS AND SUBJECT DETAILS
 - Animal Studies
- METHOD DETAILS
 - Chlorine Gas Exposure
 - Naphthalene injury model
 - SO₂ and Influenza infection induced injury
 - Tissue harvesting, sectioning, and H&E staining
 - Mouse SMG dissection and dissociation
 - Pig SMG dissection and dissociation
 - SMG cell culture and immunocytochemistry
 - SMG cell engraftment and scaffold culture
 - Section Immunohistochemistry

- Whole mount immunohistochemistry
- Image acquisition, processing and quantification
- Single cell capture and library preparation
- scRNA-seq analysis

- QUANTIFICATION AND STATISTICAL ANALYSES
- DATA AND SOFTWARE AVAILABILITY

SUPPLEMENTAL INFORMATION

Supplemental Information includes seven figures and can be found with this article online at <https://doi.org/10.1016/j.stem.2018.03.018>.

ACKNOWLEDGMENTS

We thank Brigid Hogan, Ken Poss, Don Fox, and Nellwyn Hagan for critically reading the manuscript. We thank Brigid Hogan for sharing *Acta2-creER* mice, Henry Kronenberg for *Sox9-creERT2* mice, and members of the Hogan and Barkauskas laboratories for discussions. We thank the DMPI 10X genomics core for their assistance with scRNA-seq and Brigid Hogan and Dr. Colin Bingle (The University of Sheffield, UK) for the PLUNC antibody. This research was supported by a career development award from NHLBI/NIH (4R00HL127181) to P.R.T. and funds from Regeneration NeXT Initiative at Duke University. P.R.T. is a Whitehead Scholar. Research reported in this publication is supported in part by the CounterACT Program through the National Institute of Environmental Health Sciences of the NIH under award number U01ES017219 to M.D.G.

AUTHOR CONTRIBUTIONS

A.T. designed, conceived, and performed the experiments and co-wrote the manuscript; R.D.C. performed computational analysis; Y.K., A.J.M., J.T., and A.D. performed IHC and quantified the number of cells; and T.J.M. performed and helped with the porcine injury experiments. M.D.G. supervised pig injury experiments. P.R.T. designed, conceived, and supervised the work and co-wrote the manuscript. All authors reviewed and edited the manuscript. Correspondence and requests for materials should be addressed to P.R.T.

DECLARATION OF INTERESTS

The authors declare no competing interests.

Received: September 14, 2017

Revised: February 1, 2018

Accepted: March 21, 2018

Published: April 12, 2018

REFERENCES

- Adam, R.C., Yang, H., Rockowitz, S., Larsen, S.B., Nikolova, M., Orstian, D.S., Polak, L., Kadaja, M., Asare, A., Zheng, D., and Fuchs, E. (2015). Pioneer factors govern super-enhancer dynamics in stem cell plasticity and lineage choice. *Nature* 521, 366–370.

Figure 7. SOX9-Dependent Mechanisms Are Important for the Contribution of MECs to SE Repair after Naphthalene-Induced Injury

- (A) Heatmap data from scRNA-seq analysis indicate potential SOX9 target genes that are differentially expressed in *Acta2⁺* cells in homeostatic SMGs and *Acta2⁺* cells isolated from SE following naphthalene-induced injury.
- (B) Schematic representation of experimental design to delete *Sox9* in myoepithelial cells followed by naphthalene administration to induce airway injury.
- (C) Co-IHC for ACTA2 (green), SOX9 (red), and nuclear DAPI (blue) on tracheal sections. Arrows indicate nuclei of ACTA2⁺ myoepithelial cells. The scale bar represents 20 μ m.
- (D) Quantification of SOX9-expressing cells among myoepithelial cells of *Krt5-SOX9-LOF* and *Sox9^{ff}* mice. Data are shown as mean \pm SEM ($n = 3$; *** $p \leq 0.001$).
- (E) IHC for ACTA2 (green), SOX9 (red), Ki67 (gray), and DAPI (blue) on tracheal longitudinal sections collected from *Krt5-SOX9-LOF* and *Sox9^{ff}* mice on day 4 post-naphthalene injury. The dashed line separates the SE cell layer from the mesenchyme. The scale bars represent 50 μ m.
- (F) Quantification of ACTA2⁺, SOX9⁺, and Ki67⁺ cells among total DAPI⁺ cells in SE spanning cartilage rings between 0 and 3 in naphthalene-injured mice. Data shown are mean \pm SEM ($n = 3$; * $p \leq 0.05$; ** $p \leq 0.01$).

See also Figure S7.

- Anderson, P.J., Lynch, T.J., and Engelhardt, J.F. (2017). Multipotent myoepithelial progenitor cells are born early during airway submucosal gland development. *Am. J. Respir. Cell Mol. Biol.* **56**, 716–726.
- Babbin, B.A., Parkos, C.A., Mandell, K.J., Winfree, L.M., Laur, O., Ivanov, A.I., and Nusrat, A. (2007). Annexin 2 regulates intestinal epithelial cell spreading and wound closure through Rho-related signaling. *Am. J. Pathol.* **170**, 951–966.
- Barker, N., van Es, J.H., Kuipers, J., Kujala, P., van den Born, M., Cozijnsen, M., Haeghebaert, A., Korving, J., Begthel, H., Peters, P.J., and Clevers, H. (2007). Identification of stem cells in small intestine and colon by marker gene Lgr5. *Nature* **449**, 1003–1007.
- Bingle, L., and Bingle, C.D. (2011). Distribution of human PLUNC/BPI fold-containing (BPIF) proteins. *Biochem Soc Trans* **39**, 1023–1027.
- Blanpain, C., and Fuchs, E. (2014). Stem cell plasticity. Plasticity of epithelial stem cells in tissue regeneration. *Science* **344**, 1242281.
- Borthwick, D.W., West, J.D., Keighren, M.A., Flockhart, J.H., Innes, B.A., and Dorin, J.R. (1999). Murine submucosal glands are clonally derived and show a cystic fibrosis gene-dependent distribution pattern. *Am. J. Respir. Cell Mol. Biol.* **20**, 1181–1189.
- Borthwick, D.W., Shahbazian, M., Krantz, Q.T., Dorin, J.R., and Randell, S.H. (2001). Evidence for stem-cell niches in the tracheal epithelium. *Am. J. Respir. Cell Mol. Biol.* **24**, 662–670.
- Buckpitt, A., Chang, A.M., Weir, A., Van Winkle, L., Duan, X., Philpot, R., and Plopper, C. (1995). Relationship of cytochrome P450 activity to Clara cell cytotoxicity. IV. Metabolism of naphthalene and naphthalene oxide in microdissected airways from mice, rats, and hamsters. *Mol. Pharmacol.* **47**, 74–81.
- Choi, H.K., Finkbeiner, W.E., and Widdicombe, J.H. (2000). A comparative study of mammalian tracheal mucous glands. *J. Anat.* **197**, 361–372.
- Cole, B.B., Smith, R.W., Jenkins, K.M., Graham, B.B., Reynolds, P.R., and Reynolds, S.D. (2010). Tracheal Basal cells: a facultative progenitor cell pool. *Am. J. Pathol.* **177**, 362–376.
- Crystal, R.G., Randell, S.H., Engelhardt, J.F., Voynow, J., and Sunday, M.E. (2008). Airway epithelial cells: current concepts and challenges. *Proc. Am. Thorac. Soc.* **5**, 772–777.
- Donati, G., Rognoni, E., Hiratsuka, T., Liakath-Ali, K., Hoste, E., Kar, G., Kayikci, M., Russell, R., Kretzschmar, K., Mulder, K.W., et al. (2017). Wounding induces dedifferentiation of epidermal Gata6⁺ cells and acquisition of stem cell properties. *Nat. Cell Biol.* **79**, 603–613.
- Franks, T.J., Colby, T.V., Travis, W.D., Tuder, R.M., Reynolds, H.Y., Brody, A.R., Cardoso, W.V., Crystal, R.G., Drake, C.J., Engelhardt, J., et al. (2008). Resident cellular components of the human lung: current knowledge and goals for research on cell phenotyping and function. *Proc. Am. Thorac. Soc.* **5**, 763–766.
- Gao, X., Bali, A.S., Randell, S.H., and Hogan, B.L.M. (2015). GRHL2 coordinates regeneration of a polarized mucociliary epithelium from basal stem cells. *J. Cell Biol.* **211**, 669–682.
- Ghosh, M., Helm, K.M., Smith, R.W., Giordanengo, M.S., Li, B., Shen, H., and Reynolds, S.D. (2011). A single cell functions as a tissue-specific stem cell and the in vitro niche-forming cell. *Am. J. Respir. Cell Mol. Biol.* **45**, 459–469.
- Gunnarsson, M., Walther, S.M., Seidal, T., Bloom, G.D., and Lennquist, S. (1998). Exposure to chlorine gas: effects on pulmonary function and morphology in anaesthetised and mechanically ventilated pigs. *J. Appl. Toxicol.* **18**, 249–255.
- Hegab, A.E., Kubo, H., Fujino, N., Suzuki, T., He, M., Kato, H., and Yamaya, M. (2010). Isolation and characterization of murine multipotent lung stem cells. *Stem Cells Dev.* **19**, 523–536.
- Hegab, A.E., Ha, V.L., Gilbert, J.L., Zhang, K.X., Malkoski, S.P., Chon, A.T., Darmawan, D.O., Bisht, B., Ooi, A.T., Pellegrini, M., et al. (2011). Novel stem/progenitor cell population from murine tracheal submucosal gland ducts with multipotent regenerative potential. *Stem Cells* **29**, 1283–1293.
- Hegab, A.E., Nickerson, D.W., Ha, V.L., Darmawan, D.O., and Gomperts, B.N. (2012). Repair and regeneration of tracheal surface epithelium and submucosal glands in a mouse model of hypoxic-ischemic injury. *Respirology* **17**, 1101–1113.
- Hogan, B.L.M., Barkauskas, C.E., Chapman, H.A., Epstein, J.A., Jain, R., Hsia, C.C.W., Niklason, L., Calle, E., Le, A., Randell, S.H., et al. (2014). Repair and regeneration of the respiratory system: complexity, plasticity, and mechanisms of lung stem cell function. *Cell Stem Cell* **15**, 123–138.
- Hong, K.U., Reynolds, S.D., Giangreco, A., Hurley, C.M., and Stripp, B.R. (2001). Clara cell secretory protein-expressing cells of the airway neuroepithelial body microenvironment include a label-retaining subset and are critical for epithelial renewal after progenitor cell depletion. *Am. J. Respir. Cell Mol. Biol.* **24**, 671–681.
- Hong, K.U., Reynolds, S.D., Watkins, S., Fuchs, E., and Stripp, B.R. (2004a). Basal cells are a multipotent progenitor capable of renewing the bronchial epithelium. *Am. J. Pathol.* **164**, 577–588.
- Hong, K.U., Reynolds, S.D., Watkins, S., Fuchs, E., and Stripp, B.R. (2004b). In vivo differentiation potential of tracheal basal cells: evidence for multipotent and unipotent subpopulations. *Am. J. Physiol. Lung Cell. Mol. Physiol.* **286**, L643–L649.
- Hsu, Y.-C., Pasolli, H.A., and Fuchs, E. (2011). Dynamics between stem cells, niche, and progeny in the hair follicle. *Cell* **144**, 92–105.
- Jeffery, P.K. (1991). Morphology of the airway wall in asthma and in chronic obstructive pulmonary disease. *Am. Rev. Respir. Dis.* **143**, 1152–1158, discussion 1161.
- Judge, E.P., Hughes, J.M.L., Egan, J.J., Maguire, M., Molloy, E.L., and O'Dea, S. (2014). Anatomy and bronchoscopy of the porcine lung. A model for translational respiratory medicine. *Am. J. Respir. Cell Mol. Biol.* **51**, 334–343.
- Kotton, D.N., and Morrisey, E.E. (2014). Lung regeneration: mechanisms, applications and emerging stem cell populations. *Nat. Med.* **20**, 822–832.
- Kuleshov, M.V., Jones, M.R., Rouillard, A.D., Fernandez, N.F., Duan, Q., Wang, Z., Koplev, S., Jenkins, S.L., Jagodnik, K.M., Lachmann, A., et al. (2016). Enrichr: a comprehensive gene set enrichment analysis web server 2016 update. *Nucleic Acids Res.* **44** (W1), W90–W97.
- Liu, X., and Engelhardt, J.F. (2008). The glandular stem/progenitor cell niche in airway development and repair. *Proc. Am. Thorac. Soc.* **5**, 682–688.
- Liu, J.Y., Nettesheim, P., and Randell, S.H. (1994). Growth and differentiation of tracheal epithelial progenitor cells. *Am. J. Physiol.* **266**, L296–L307.
- Merrell, A.J., and Stanger, B.Z. (2016). Adult cell plasticity in vivo: de-differentiation and transdifferentiation are back in style. *Nat. Rev. Mol. Cell Biol.* **17**, 413–425.
- Mou, H., Vinarsky, V., Tata, P.R., Brazauskas, K., Choi, S.H., Crooke, A.K., Zhang, B., Solomon, G.M., Turner, B., Bihler, H., et al. (2016). Dual SMAD signaling inhibition enables long-term expansion of diverse epithelial basal cells. *Cell Stem Cell* **19**, 217–231.
- Nabhan, A., Brownfield, D.G., Harbury, P.B., Krasnow, M.A., and Desai, T.J. (2018). Single-cell Wnt signaling niches maintain stemness of alveolar type 2 cells. *Science*, eaam6603.
- Noritake, J., Watanabe, T., Sato, K., Wang, S., and Kaibuchi, K. (2005). IQGAP1: a key regulator of adhesion and migration. *J. Cell Sci.* **118**, 2085–2092.
- O'Koren, E.G., Hogan, B.L.M., and Gunn, M.D. (2013). Loss of basal cells precedes bronchiolitis obliterans-like pathological changes in a murine model of chlorine gas inhalation. *Am. J. Respir. Cell Mol. Biol.* **49**, 788–797.
- Pardo-Saganta, A., Tata, P.R., Law, B.M., Saez, B., Chow, R.D.-W., Prabhu, M., Gridley, T., and Rajagopal, J. (2015a). Parent stem cells can serve as niches for their daughter cells. *Nature* **523**, 597–601.
- Pardo-Saganta, A., Law, B.M., Tata, P.R., Villoria, J., Saez, B., Mou, H., Zhao, R., and Rajagopal, J. (2015b). Injury induces direct lineage segregation of functionally distinct airway basal stem/progenitor cell subpopulations. *Cell Stem Cell* **16**, 184–197.
- Prater, M.D., Petit, V., Alasdair Russell, I., Giraddi, R.R., Shehata, M., Menon, S., Schulte, R., Kalajzic, I., Rath, N., Olson, M.F., et al. (2014). Mammary stem cells have myoepithelial cell properties. *Nat. Cell Biol.* **16**, 942–950.
- Rajagopal, J., and Stanger, B.Z. (2016). Plasticity in the adult: how should the Waddington diagram be applied to regenerating tissues? *Dev. Cell* **36**, 133–137.

- Rios, A.C., Fu, N.Y., Lindeman, G.J., and Visvader, J.E. (2014). *In situ* identification of bipotent stem cells in the mammary gland. *Nature* 506, 322–327.
- Rock, J.R., Onaitis, M.W., Rawlins, E.L., Lu, Y., Clark, C.P., Xue, Y., Randell, S.H., and Hogan, B.L.M. (2009). Basal cells as stem cells of the mouse trachea and human airway epithelium. *Proc. Natl. Acad. Sci. USA* 106, 12771–12775.
- Rock, J.R., Gao, X., Xue, Y., Randell, S.H., Kong, Y.-Y., and Hogan, B.L.M. (2011). Notch-dependent differentiation of adult airway basal stem cells. *Cell Stem Cell* 8, 639–648.
- Rompolas, P., Mesa, K.R., and Greco, V. (2013). Spatial organization within a niche as a determinant of stem-cell fate. *Nature* 502, 513–518.
- Scadden, D.T. (2014). Nice neighborhood: emerging concepts of the stem cell niche. *Cell* 157, 41–50.
- Simionescu-Bankston, A., Leoni, G., Wang, Y., Pham, P.P., Ramalingam, A., DuHadaway, J.B., Faundez, V., Nusrat, A., Prendergast, G.C., and Pavlath, G.K. (2013). The N-BAR domain protein, Bin3, regulates Rac1- and Cdc42-dependent processes in myogenesis. *Dev. Biol.* 382, 160–171.
- Soeda, T., Deng, J.M., de Crombrugge, B., Behringer, R.R., Nakamura, T., and Akiyama, H. (2010). Sox9-expressing precursors are the cellular origin of the cruciate ligament of the knee joint and the limb tendons. *Genesis* 48, 635–644.
- Stange, D.E., Koo, B.-K., Huch, M., Sibbel, G., Basak, O., Lyubimova, A., Kujala, P., Bartfeld, S., Koster, J., Geahlen, J.H., et al. (2013). Differentiated Troy+ chief cells act as reserve stem cells to generate all lineages of the stomach epithelium. *Cell* 155, 357–368.
- Stripp, B.R., Maxson, K., Mera, R., and Singh, G. (1995). Plasticity of airway cell proliferation and gene expression after acute naphthalene injury. *Am. J. Physiol.* 269, L791–L799.
- Tata, P.R., and Rajagopal, J. (2016). Cellular plasticity: 1712 to the present day. *Curr. Opin. Cell Biol.* 43, 46–54.
- Tata, P.R., and Rajagopal, J. (2017). Plasticity in the lung: making and breaking cell identity. *Development* 144, 755–766.
- Tata, P.R., Mou, H., Pardo-Saganta, A., Zhao, R., Prabhu, M., Law, B.M., Vinarsky, V., Cho, J.L., Breton, S., Sahay, A., et al. (2013). Dedifferentiation of committed epithelial cells into stem cells *in vivo*. *Nature* 503, 218–223.
- Tetteh, P.W., Farin, H.F., and Clevers, H. (2015). Plasticity within stem cell hierarchies in mammalian epithelia. *Trends Cell Biol.* 25, 100–108.
- van der Maaten, L. (2014). Accelerating t-SNE using tree-based algorithms. *J. Mach. Learn. Res.* 15, 3221–3245.
- van Es, J.H., Sato, T., van de Wetering, M., Lyubimova, A., Yee Nee, A.N., Gregoriet, A., Sasaki, N., Zeinstra, L., van den Born, M., Korving, J., et al. (2012). Dll1+ secretory progenitor cells revert to stem cells upon crypt damage. *Nat. Cell Biol.* 14, 1099–1104.
- Van Keymeulen, A., Rocha, A.S., Ousset, M., Beck, B., Bouvencourt, G., Rock, J., Sharma, N., Dekoninck, S., and Blanpain, C. (2011). Distinct stem cells contribute to mammary gland development and maintenance. *Nature* 479, 189–193.
- Van Winkle, L.S., Buckpitt, A.R., Nishio, S.J., Isaac, J.M., and Plopper, C.G. (1995). Cellular response in naphthalene-induced Clara cell injury and bronchiolar epithelial repair in mice. *Am. J. Physiol.* 269, L800–L818.
- Vicente-Manzanares, M., Ma, X., Adelstein, R.S., and Horwitz, A.R. (2009). Non-muscle myosin II takes centre stage in cell adhesion and migration. *Nat. Rev. Mol. Cell Biol.* 10, 778–790.
- Visvader, J.E., and Clevers, H. (2016). Tissue-specific designs of stem cell hierarchies. *Nat. Cell Biol.* 18, 349–355.
- Wang, J., Winskog, C., Edston, E., and Walther, S.M. (2005). Inhaled and intravenous corticosteroids both attenuate chlorine gas-induced lung injury in pigs. *Acta Anaesthesiol. Scand.* 49, 183–190.
- Wansleeben, C., Bowie, E., Hotten, D.F., Yu, Y.-R.A., and Hogan, B.L.M. (2014). Age-related changes in the cellular composition and epithelial organization of the mouse trachea. *PLoS ONE* 9, e93496.
- Wendling, O., Bornert, J.-M., Chambon, P., and Metzger, D. (2009). Efficient temporally-controlled targeted mutagenesis in smooth muscle cells of the adult mouse. *Genesis* 47, 14–18.
- Xiong, G.P., Zhang, J.X., Gu, S.P., Wu, Y.B., and Liu, J.F. (2012). Overexpression of ECM1 contributes to migration and invasion in cholangiocarcinoma cell. *Neoplasma* 59, 409–415.
- Zacharias, W.J., Frank, D.B., Zepp, J.A., Morley, M.P., Alkhaleel, F.A., Kong, J., Zhou, S., Cantu, E., and Morrisey, E.E. (2018). Regeneration of the lung alveolus by an evolutionarily conserved epithelial progenitor. *Nature* 555, 251–255.
- Zhu, S., Zhang, X., Weichert-Leahy, N., Dong, Z., Zhang, C., Lopez, G., Tao, T., He, S., Wood, A.C., Oldridge, D., et al. (2017). LMO1 synergizes with MYCN to promote neuroblastoma initiation and metastasis. *Cancer Cell* 32, 310–323.e5.

STAR★METHODS

KEY RESOURCES TABLE

REAGENT or RESOURCE	SOURCE	IDENTIFIER
Antibodies		
Rabbit polyclonal to Aquaporin 3	Abcam	Ab125219
Rabbit Polyclonal anti-alpha SMA	Abcam	Ab5694;
Mouse Monoclonal anti-alpha SMA	Sigma-Aldrich	A2547 RRID:AB_476701
Rat Monoclonal anti-KRT8	DSHB	TROMA-I RRID:AB_531826
Rabbit Polyclonal anti-KRT5	Abcam	Ab53121 RRID:AB_869889
Mouse Monoclonal anti-KRT14	ThermoFisher	MS-115-P1;
Rabbit Polyclonal anti-Ki67	Abcam	Ab15580; RRID:AB_443209
Rabbit Polyclonal anti-P63	Genetex	GTX102425 RRID:AB_1952344
Rat Monoclonal anti-Ki67	ThermoFisher	14-5698-82 RRID:AB_10854564
Mouse Monoclonal anti-TP63	OriGene	TA802078 RRID:AB_2626201
Rabbit Polyclonal anti-Sox9	Millipore	Ab5535 RRID:AB_2239761
Mouse Monoclonal anti-Sox9	Abcam	Ab76997 RRID:AB_2194156
Mouse Monoclonal anti-Acetylated tubulin	ProteinTech	66200-1-Ig
Rat monoclonal anti-E-cadherin	Innovative Research	13-1900 RRID:AB_86571
Goat polyclonal CC10	Santa Cruz	Sc-9772 RRID:AB_2238819
Rabbit polyclonal Plunc	Bingle and Bingle, 2011	kindly provided by Dr. Colin Bingle (The University of Sheffield, U.K.)
Rabbit polyclonal NGFR	Abcam	Ab8875 RRID:AB_306828
Rat monoclonal Integrin alpha 6	R&D	MAB13501 RRID:AB_2128311
Anti-UEA1	Vector Laboratories	RL-1062 RRID:AB_2336769
Mouse Anti-SSEA1	DSHB	MC-480 RRID:AB_528475
Rabbit Polyclonal anti-Lactotransferrin	Millipore	07-685 RRID:AB_11211872
Rabbit Polyclonal ZO-1	Abcam	Ab216880
Alexa Fluoro 488 Donkey anti-mouse IgG	Invitrogen	A21202 RRID:AB_141607
Alexa Fluoro 594 Donkey anti-mouse IgG	Invitrogen	A21203 RRID:AB_141633
Alexa Fluoro 647 Donkey anti-mouse IgG	Invitrogen	A31571 RRID:AB_162542
Alexa Fluoro 488 Donkey anti-rabbit IgG	Invitrogen	A21206 RRID:AB_141708
Alexa Fluoro 594 Donkey anti-rabbit IgG	Invitrogen	A21207 RRID:AB_141637
Alexa Fluoro 647 Donkey anti-rabbit IgG	Invitrogen	A31573 RRID:AB_2536183
Alexa Fluoro 488 Donkey anti-goat IgG	Invitrogen	A11055 RRID:AB_142672
Alexa Fluoro 594 Donkey anti-goat IgG	Invitrogen	A11058 RRID:AB_142540
Alexa Fluoro 647 Donkey anti-goat IgG	Invitrogen	A21447 RRID:AB_141844
Alexa Fluoro 488 Donkey anti-rat IgG	Invitrogen	A21208 RRID:AB_141709
Alexa Fluoro 594 Donkey anti-rat IgG	Invitrogen	A21209 RRID:AB_2535795
Chemicals, Peptides, and Recombinant Proteins		
Y-27632 2HCl ROCK1 (p160ROCK inhibitor)	Selleckchem	S1049
DMH-1 (BMP antagonist)	Tocris	4126
CHIR 99021 (Wnt agonist)	Tocris	4423
A 83-01 (TGF antagonist)	Tocris	2939
Small Airway Epithelial Cell Growth Medium (SAGM)	Lonza	CC-3118
BulletKit		
PneumaCult-ALI Medium	STEMCELL technologies	05001
Matrigel	Corning	356230
Dulbecco's Modification of Eagle's Medium (DMEM)	Corning	10-013-CV

(Continued on next page)

Continued

REAGENT or RESOURCE	SOURCE	IDENTIFIER
PBS	Genesee Scientific	25-507
MgCl ₂	Sigma	M4880
NaCl	Sigma	S9888
KCl	Invitrogen	AM9640G
CaCl ₂	Sigma	C5670
HEPES	GIBCO	15630080
Bovine Albumin Fraction V (7.5% solution)	GIBCO	15260037
Cellstripper	Corning	25-056-CI
Hyaluronidase from bovine testes type I-S	Sigma	H3506-500MG
Collagenase, Type II, powder	GIBCO	17101-015
Collagenase, Type I, powder	GIBCO	17100017
Trypsin-EDTA (0.25%), phenol red	GIBCO	25200056
Penicillin-Streptomycin (10,000 U/mL)	GIBCO	15140122
Antibiotic-Antimycotic (100X)	GIBCO	15240062
Gentamycin sulfate	Sigma	G1914
Paraformaldehyde solution 4% in PBS	Santa Cruz	sc-281692
Tamoxifen	Sigma	T5648-1G
Bovine Serum Albumin	Sigma-Aldrich	A7906
O.C.T. Compound	Fisher Scientific	23-730-571
Citrate Buffer 10x	Sigma-Aldrich	C9999
Sucrose	Sigma-Aldrich	S0389
Triton X-100	Sigma-Aldrich	X100
Fluoromount-G, with DAPI	Thermo Fisher Scientific	00-4959
Deposited Data		
Airway surface and submucosal gland scRNA-seq	This paper	GEO: GSE111598
Experimental Models: Organisms/Strains		
C57BL/6J	The Jackson Laboratory	Jax # 000664
CD-1 IGS	Charles river	CRL# 022
Sox9 ^{tm1(cre/ERT2)Haak}	Soeda et al., 2010	N/A
Tg(Acta2-cre/ERT2)12Pcn	Hogan lab Wendling et al., 2009	N/A
Krt5tm1.1(cre/ERT2)Blh	The Jackson Laboratory	Jax# 029155
B6.129S7-Sox9 ^{tm2Crm} /J	The Jackson Laboratory	Jax# 013106
B6.Cg-Gt(ROSA)26Sor ^{tm9(CAG-tdTomato)Hze} /J	The Jackson Laboratory	Jax# 007909
American Yorkshire pigs	Looper Farms, Granite Falls, NC	
Software and Algorithms		
ImageJ	NIH	N/A
10x Genomics Cell Ranger	10X Genomics	N/A
R Studio	N/A	N/A
Python	N/A	N/A
Enrichr	Kuleshov et al., 2016	http://amp.pharm.mssm.edu/Enrichr/

CONTACT FOR REAGENTS AND RESOURCE SHARING

Further information and requests for resource/reagents should be directed to and will be fulfilled by the Lead Contact, Purushothama Rao Tata (purushothamarao.tata@duke.edu)

EXPERIMENTAL MODELS AND SUBJECT DETAILS

Animal Studies

All laboratory mice were maintained under standard husbandry and housing conditions approved by the Duke University Institutional Animal Care and Use Committee. All animals were handled in accordance with the NIH and AAALAC guidelines for humane care and use of laboratory animals. Mice used for experiments were not involved in previous procedures and were drug or test naive. Mice were kept in a SPF breeding area under specified pathogen free conditions. Cages, bedding, food and water were autoclaved. Animals were maintained on the same 12 h light/dark cycle and monitored daily by caretakers and researchers. Health monitoring did not reveal any infections in the past 18 months. Male and female C57BL/6J, CD-1, and transgenic mice aged 6-12 weeks were used for experiments with similar aged mice for both control and treatment groups. *Sox9-creERT2* (Soeda et al., 2010); (kindly provided by Henry Kronenberg, MGH, Boston) were bred with *R26R-tdTomato* mice (Jackson Laboratory 007914) to generate *Sox9-creERT2::R26R-tdTomato* males, which were then crossed with C57BL/6 or CD-1 to generate experimental animals. *Acta2-creERT2* (kindly provided by Hogan lab, Duke University; (Wendling et al., 2009)) females were bred with *R26R-tdTomato* (homozygous) males to obtain *Acta2-creERT2-R26R-tdTomato* and maintained on a C57BL/6 background. To label *Sox9* or *Acta2*-expressing cells, 3 doses of tamoxifen were administered intraperitoneally (2mg/20 gms body weight) to induce *cre recombinase* mediated excision of a stop codon and subsequent expression of *tdTomato*. Mice were allowed to recover for 4 weeks between tamoxifen treatment and naphthalene injury. *Krt5-creERT2* (Jackson Laboratory 029155) were bred with *Sox9^{f/f}* (Jackson Laboratory 013106) to generate *Krt5-creERT2;Sox9^{f/f}* males, which were then crossed to *Sox9^{f/f}* females to generate experimental animals. *Krt5-CreERT2::Sox9^{f/f}* and *Sox9^{f/f}* littermates were maintained on a C57BL/6j background. *Krt5-creERT2;Sox9^{f/f}* and *Sox9^{f/f}* mice were given five doses of tamoxifen (2mg/20 gms body weight) followed by an interval of 3 weeks prior to naphthalene administration.

Domestic, juvenile American Yorkshire pigs (30-40 kg) of both sexes were obtained from a certified specific pathogen free breeder (Looper Farms, Granite Falls, NC). The animals were housed for an acclimation period in an adjoining facility for a minimum of 24 h prior to all studies. Animals were pre-medicated with ketamine (22 mg/kg IM) and acepromazine (1.1 mg/kg IM). Following pre-medication, propofol was administered as a single bolus (5-10 mg/kg IV) to facilitate tracheal intubation, and then continuously (5-10 mg/kg/hr IV) during mechanical ventilation. All animals were volume-control ventilated (AVEA, CareFusion Inc., Yorba Linda, CA) with a tidal volume of 7 ml/kg, a respiratory rate of 25 breaths per minute, and PEEP set to 5 cm H₂O. Initial FiO₂ was 0.21 and adjusted as needed to maintain SpO₂ ≥ 90%. No further changes to the ventilator settings were made for the duration of experiments. Following chlorine or filtered air exposure, propofol was halted and replaced with an isotonic crystalloid solution (4 ml/kg/hr IV). Animals were weaned from mechanical ventilation until sustained spontaneous breathing was observed. Animals were returned to their enclosure and closely observed until upright. Animals were then monitored for 48 h for signs of respiratory distress, with heart rate and oxygenation saturation measured during voluntary feeding. After 48 h, animals were humanely euthanized while under deep anesthesia with potassium chloride (4-10 mmol/kg IV).

METHOD DETAILS

Chlorine Gas Exposure

Chlorine gas exposure and evacuation was performed according to a protocol approved by the Duke University Occupational & Environmental Safety Office. After animals were stably ventilated for 30 min to ensure appropriate sedation and analgesia, chlorine gas exposure was initiated by opening a valve on the inspiratory limb of the ventilator circuit. Compressed chlorine gas from a calibrated cylinder (Airgas National Welders, Durham, NC) was delivered via a 2-stage regulator through an adjustable flowmeter (Cole-Parmer) for 30 min at a concentration of 170 ± 8 ppm, with intermittent monitoring of the chlorine gas concentration (PortaSens II, Analytical Technology Inc., Collegeville, PA) to ensure consistent levels of exposure. Residual chlorine gas was scavenged under 100% vacuum of the exhaled breath via the unidirectional expiratory line of the ventilator circuit through a series of wet-scrubbing containment flasks containing 10% NaOH. As an additional safeguard, the animals and the ventilator circuit were placed under a negative pressure chamber with colorimetric indicators (Morphix Technologies) for the detection of leaked chlorine gas. These experiments are performed on two independent pigs.

Naphthalene injury model

Naphthalene administration was performed following standard procedures as described previously (Hong et al., 2001). Briefly, a single dose of naphthalene (dissolved in corn oil) was administered intraperitoneally at 275 mg/kg body weight to induce injury. Naphthalene is toxic and causes skin and eye irritation. So, care must be taken while preparing the reagent. Groups of 3-4 mice were sacrificed on day 1, 3, 5, 10, 12, 20, 60, and 80 post naphthalene and trachea were dissected. Corn oil administered mice served as vehicle control. Freshly prepared naphthalene was administered between 7:00 A.M. - 8:00 A.M.. Inconsistent injury was observed if administered later in the day or using frozen aliquots of naphthalene. No blinding was used, and no data was excluded from the analysis.

SO₂ and Influenza infection induced injury

SO₂ exposure and influenza infection was performed as previously described (Tata et al., 2013). Briefly, mice were placed in a chambered cage which was placed in a transparent polystyrene chamber. Compressed SO₂ gas from a calibrated cylinder (Airgas Inc.)

was delivered via a 2-stage regulator through an adjustable flowmeter for 3h 40 min at a concentration of 500ppm of SO₂, with intermittent monitoring of the SO₂ gas concentration to ensure consistent levels of exposure. Control mice were exposed to filtered air under otherwise the same conditions. After exposure, mice were returned to their cages where they received atmospheric air. For influenza-induced injury experiments, mice were anesthetized using ketamine/xylazine. Influenza virus A/Puerto Rico/8/34 (PR8) (kindly provided by Dr. Nicholas Heaton, Duke University) dose was determined based on titration experiments. Mice were anesthetized and administered 10³ PFU virus, which was determined to result in a LD value of 75, through intranasal inhalation as previously described (Tata et al., 2013). Mice health was monitored every day. Mice were sacrificed on day-1, 3, and 5 post exposure/infection, and the trachea were harvested for histological analysis. No blinding was used and no data was excluded from the analysis. These experiments are performed on three independent mice.

Tissue harvesting, sectioning, and H&E staining

Mouse trachea were harvested and fixed in 4% PFA in PBS for 30 min at RT and then washed in PBS followed by overnight incubation in 30% sucrose at 4°C. Trachea were then incubated with 1:1 mixture of 30% sucrose (in PBS)/O.C.T. for 30 min at 4°C, embedded in O.C.T. and cryosectioned (6µm). Pig trachea were harvested and fixed overnight in 10% normal buffered formalin at 4°C before paraffin embedding. 5 µm thick sections were used for histological analysis.

Mouse SMG dissection and dissociation

Trachea were dissected from tamoxifen administered *Acta2- tdt* mice and placed in DMEM+pen/strep and cut in half (around cartilage 5) and opened through the trachea lumen. Tracheal pieces were incubated in 16U/ml dispase (in DMEM+pen/strep) for 30 min at RT. Digestion was stopped using 5%FBS DMEM+pen/strep. SE was manually peeled off with forceps. Tracheal pieces were washed 3 times in DMEM+pen/strep then SMG were manually dissected with forceps, washed once with PBS, spun down at 1000 g for 2 min and incubated with collagenase II/Hyaluronidase enzyme mix (in DMEM+pen/strep) for 30 min at 37°C. Then Trypsin-EDTA was added to a final concentration of 0.1% and incubated for an additional 20 min. The enzymatic digestion was stopped with 5% FBS in DMEM+pen/strep. The suspension was filtered through a 40 µM cell strainer and spun down at 1000 g for 2 min. Cell pellet was reconstituted in SAGM media containing pen/strep, 1 µM A83-01, 10 µM Y-27632, 1 µM DMH-1, 1 µM CHIR 99021 and cultured at 37°C, 5% CO₂. Media was changed every other day between day-1 to 4 and every day after day-4 (Mou et al., 2016).

Pig SMG dissection and dissociation

Porcine tracheas were obtained from local slaughterhouse, with permission from the North Carolina Department of Agriculture and Consumer Services. Fresh trachea were transported in ice cold DMEM. Tracheal pieces were dipped in 95% ethanol for 10 s and placed in DMEM+pen/strep. SMG were manually dissected under microscope, washed once in PBS and incubated in solution containing: 110 mM NaCl, 5 mM KCl, 1 mM MgCl₂ and 2 mM CaCl₂, 20mM HEPES, 10 mg/mL of Bovine Albumin Fraction V, 200 U/mL Collagenase I, 200 U/mL collagenase II, 200 U/mL Hyaluronidase in DMEM for 1h at 37°C with gentle agitation. Samples were spun at 500 g for 2 min and cell pellet was digested for 30 min. Samples were spun down, washed once with PBS, and incubated in 0.1% Trypsin-EDTA/DMEM for 20 min. Enzymatic digestion was stopped by addition of 5% FBS/DMEM. The suspension was filtered through a 40 µM cell strainer and spun down at 1000 g for 2 min. Cells were reconstituted and cultured in SAGM media containing anti/anti, gentamycin, 1 µM A83-01, 10 µM Y-27632, 1 µM DMH-1, 1 µM CHIR 99021, 0.5% matrigel. Cells were cultured in triplicates and was repeated on three independent tracheal cells.

SMG cell culture and immunocytochemistry

Cells isolated from SMG were grown on coverslips. Cells were fixed in 4% PFA for 15 min, washed twice for 5 min in PBS, and permeabilized for 10 min in PBT (PBS + 0.1% Triton X-100). The samples were then incubated for 30 min in 1%BSA in PBT, incubated with primary antibodies at RT for 1h, washed three times for 5 min in PBT and incubated with secondary antibody for 1h at RT. Cells were washed and coverslips were mounted on slides using Fluor G reagent with DAPI. No blinding was used and no data was excluded from the analysis.

Cells were cultured in triplicates and was repeated on three independent tracheal cells.

SMG cell engraftment and scaffold culture

Trachea from C57BL/6 mice were dissected, cut in half longitudinally and trimmed to eliminate the region that contains SMGs (larynx to cartilage 3). Tracheal pieces were washed once in PBS and incubated with Cellstripper (Corning) over night at 37°C with continuous rotation to denude the SE. Next day, tracheal pieces were washed once in 10% FBS/ DMEM, twice in PBS and placed on soaked Gelfoam (Pfizer). SMG cells isolated from *Acta2- tdt* mice were expanded for 5 days prior to grafting on denuded tracheal pieces. Scaffolds were cultured in an *air-liquid-interface* in PneumaCult-ALI media for 30 days prior to histological analysis. The data presented in the results section was obtained from 7 successfully transplanted scaffolds out of 12 scaffolds engrafted. Engraftment efficiency was determined based on tdtomato expression on the scaffold surface.

Section Immunohistochemistry

Antigen retrieval was performed using 10 mM sodium citrate buffer in antigen retrieval system (Electron Microscopy Science) or water bath (90°C for 10 min). Cryosections (6 µm) were washed in PBS, permeabilized with 0.1% Triton X-100 in PBS (PBT), blocked in 1% BSA in PBT for 30 min at RT. Incubation with primary antibodies (see key resource table) was performed for 1 h at RT. Next, slides were washed 3x5 min in PBT, incubated with appropriate secondary antibodies in blocking buffer for 1h at RT, washed 3x5 min PBT and mounted using Fluor G reagent with DAPI. 5-7 µm paraffin embedded pig tissue sections were dewaxed, rehydrated before anti-body staining. Immunostaining was performed on at least 3 sections from each trachea and this was repeated on 3-5 mice.

Whole mount immunohistochemistry

Antigen retrieval was performed in 95°C (water bath) for 15 min. Next, tissues were washed with PBS, permeabilized, blocked in 1.5% BSA 0.3% Triton in PBS (1.5% BSA 0.3% PBT) for 45 min at RT and incubated over night with primary antibody in blocking solution at 37°C. Next, samples were washed 3x1h in PBT, blocked in 1.5% BSA 0.3% PBT for 45 min at RT, and incubated with secondary antibody and DAPI in blocking solution at 37°C for 45 min. After three washes in PBT tissue was mounted on slides. Immunostaining was performed at least on 3-5 mice trachea.

Image acquisition, processing and quantification

Images were captured using Olympus Confocal Microscope FV3000 using a 20X, 40X or 60X objective (all images except Figure 5A) or a Zeiss wide-field fluorescence microscope (Figure 5A). Cells were manually counted based on IHC markers and DAPI. Images were processed using Olympus CellSens application or ImageJ and figures were prepared using Affinity Designer. Large panels shown in Figures 2C, 3B, and 4B and Figures S1C, S2D, and S2G were generated by aligning and stitching single pictures using Affinity designer.

Single cell capture and library preparation

Cell suspensions at a density of 1000 cells/µl in PBS + 0.04% BSA were prepared for single cell sequencing using the Chromium Single Cell 3' Reagent Version 1 Kit and Chromium Controller (10x Genomics, CA, USA) as previously described. Briefly, 20,000 cells per reaction were loaded for GEM (Gel Bead-in-Emulsion) generation and barcoding. GEM-RT was performed using a Thermocycler. Post GEM-RT cleanup and cDNA amplification was performed to isolate and amplify cDNA for library construction. Libraries were constructed using the Chromium Single Cell 3' Reagent Kit (10x Genomics, CA, USA) and sample was sequenced in a single lane using the Illumina Nextseq 500 in Rapid Run Mode using a paired end flow cell. Read1: 26 cycles, Index2: 8 cycles, and Read2: 96 cycles.

scRNA-seq analysis

Raw Illumina sequencing output were processed through the 10x Genomics Cell Ranger software suite using default settings. Reads were mapped to the mm10 transcriptome. Read counts were normalized to \log_2 reads per million mapped (rpm) and a cutoff of \log_2 rpm ≥ 1 was used as a cutoff to determine whether a given gene was expressed in a cell.

To ensure that epithelial cells were included in the dataset, we first included any cell that expressed *Epcam*, *Cdh1*, *Krt5*, *Krt8*, or *Krt14*. We then removed endothelial cells, blood cells and macrophages by filtering out those expressing *Esam*, *H2-ab1*, *H2-aa*, *Hba-a2*, *Hbb-bt*, or *Cd68*. 139 cells were retained for further analysis. Any genes with fewer than 10 reads across the dataset were also removed from further consideration.

K-means clustering was performed in R using the *stats* package, followed by t-SNE visualization with the *Rtsne* package. Differential expression analysis was performed using edgeR in a one-versus-others approach, with a cutoff of $FDR < 0.05$ and $\log FC \geq 1$. Select differentially expressed genes were chosen for visualization in the heatmap, which was created by the *NMF* R package. Selection of *Acta2*⁺ cells was determined using a cutoff of \log_2 rpm ≥ 1 . Enrichr (amp.pharm.mssm.edu/Enrichr/) was used to perform gene ontology, pathway analysis, and genomic and proteomic interaction analysis (Kuleshov et al., 2016).

QUANTIFICATION AND STATISTICAL ANALYSES

The number of biological and technical replicates and animals are indicated in figure legends and text. Both male and female mice were used and all tested animals were included in data analysis. Briefly, the gender and mice strains used are: a) For quantitative analysis of ACTA2, SOX9 and Ki67 markers in WT (C57BL/6j) mice we used- 1 male and 2 females for controls, 3 females were used for naph-day 1, 3, and 5; b) For Acta2-tdt lineage tracing experiments- 1 male and 2 females for controls, 3 females for day-5 naphthalene, 3 females for naph-day12, 1 male and 2 females for naph-day 20, 3 females for naph-day 60 (C57BJ/6j). c) For Sox9-Tdt lineage tracing experiments- 1 male and 2 females for controls, 3 females for naph-day 5, 3 females for naph-day10 (mixed background), 3 females for naph-day 20, 1 male and 3 females for naph day 80 (C57BL/6j).

Sample size was not predetermined. Data are presented as means with standard error (SEM) to indicate the variation within each experiment. We used D'Agnostino and Pearson omnibus normality test available in Prism to test whether our data are normally distributed. All data except Figures 2D, 2E, 3F (SCGB1A1 only), S2E–S2G (ACTA2 and SOX9 only) and S2I, 7F (Sox9 only), and

S4D showed Gaussian distribution. We used Mann Whitney statistical test for non-normal distributions. Statistical differences between samples were assessed with Student two-tailed t test calculated in Excel. *p*-values below 0.05 are considered significant (**p ≤ 0.001, **p ≤ 0.01, *p ≤ 0.05).

DATA AND SOFTWARE AVAILABILITY

All relevant data are available from authors. All the software used in this work are described in the relevant methods sections. scRNA-seq data have been deposited (GEO: GSE111598).

Supplemental Information

Myoepithelial Cells of Submucosal Glands Can Function as Reserve Stem Cells to Regenerate Airways after Injury

Aleksandra Tata, Yoshihiko Kobayashi, Ryan D. Chow, Jasmine Tran, Avani Desai, Abdull J. Massri, Timothy J. McCord, Michael Dee Gunn, and Purushothama Rao Tata

Figure S1. Related to Figure 1 and Figure 2

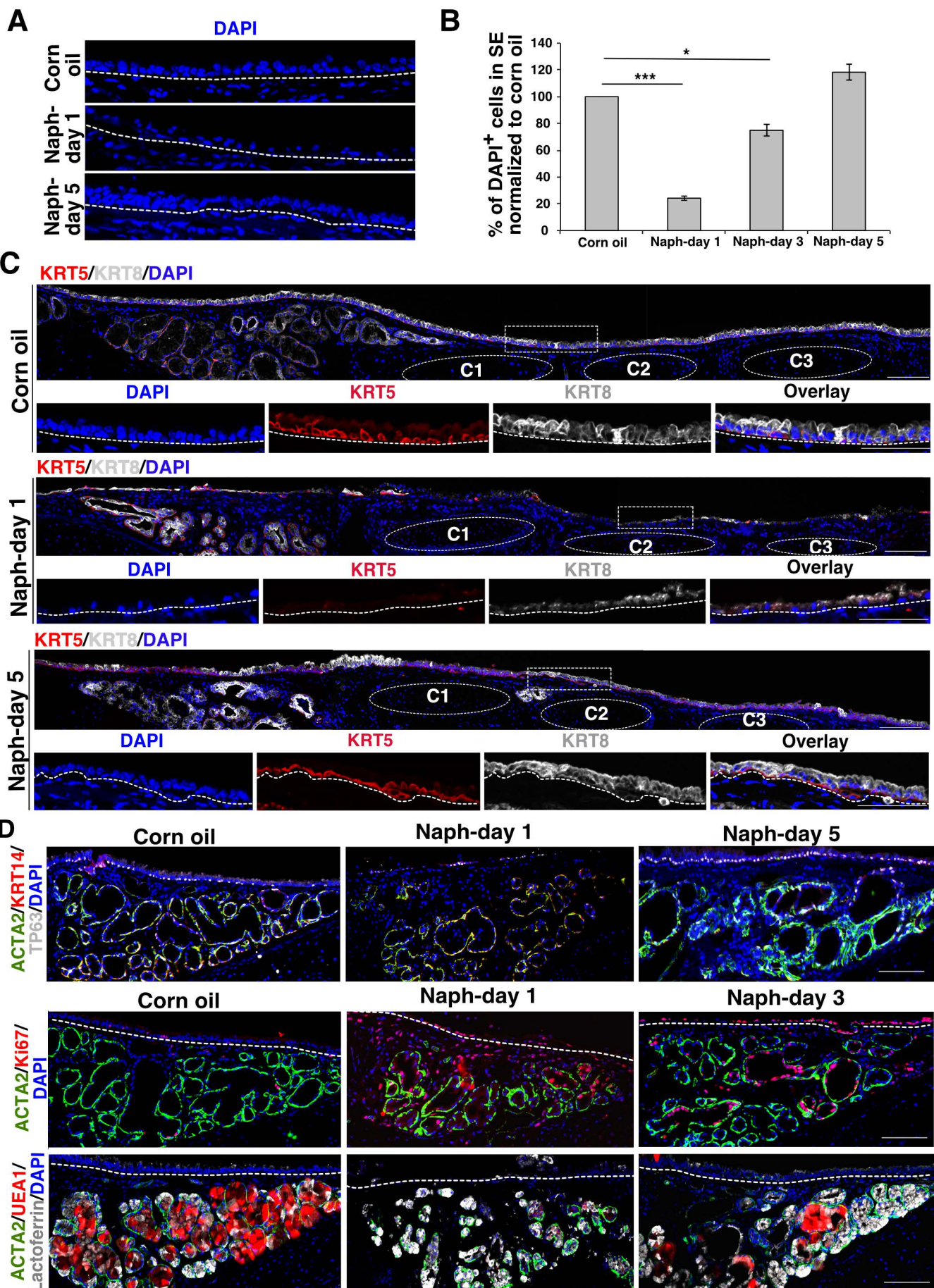


Figure S2. Related to Figure 2

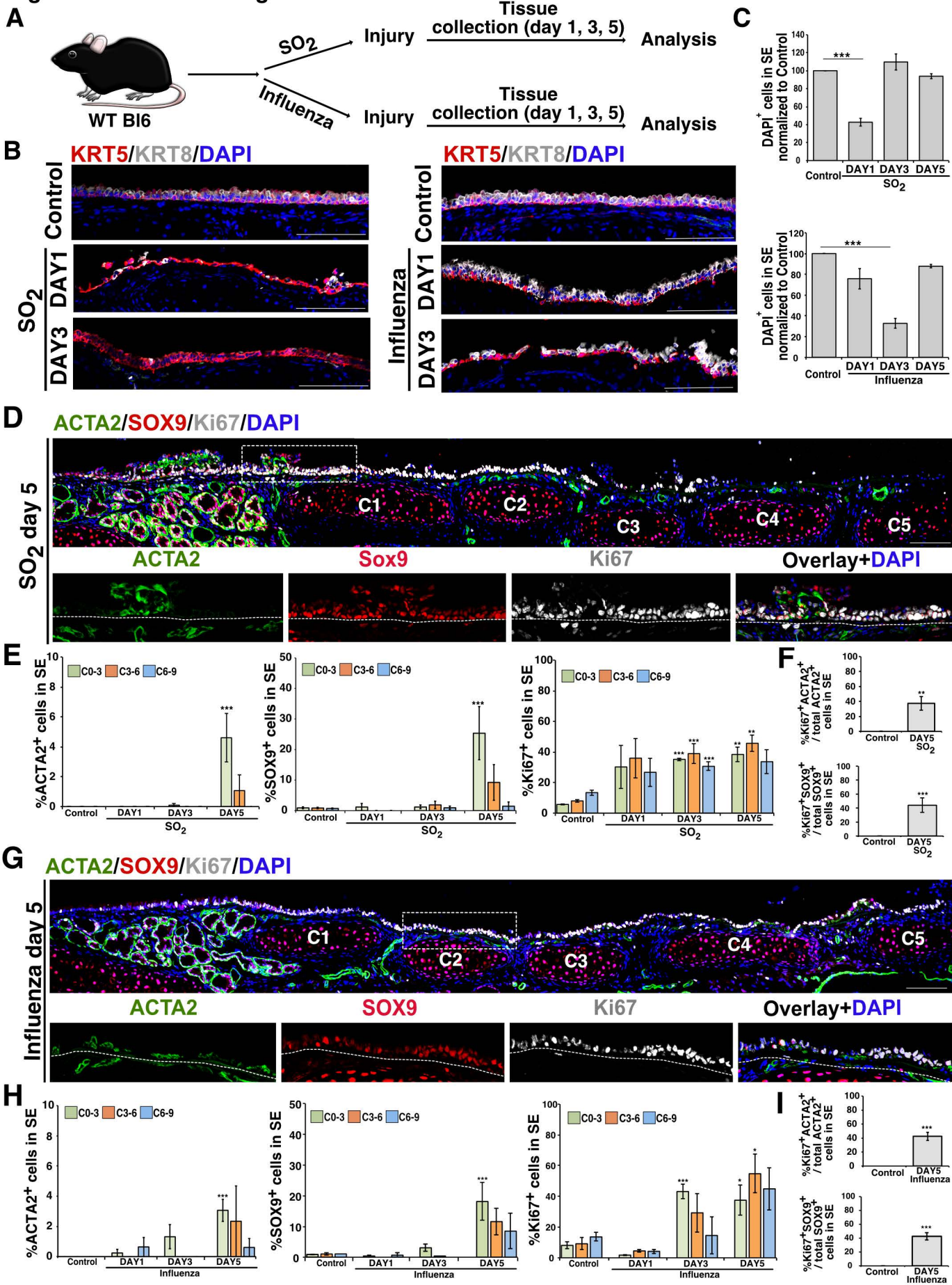


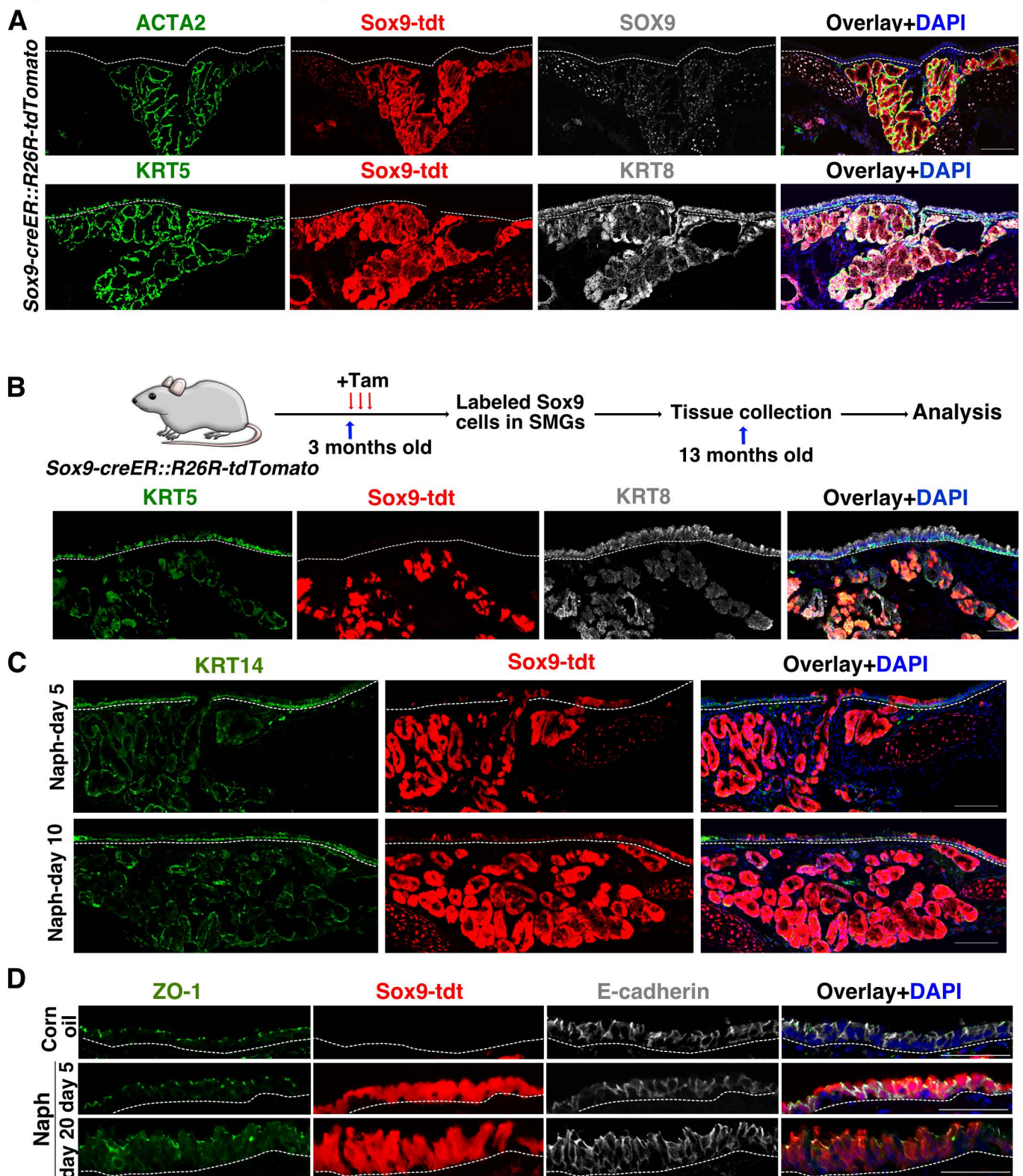
Figure S3. Related to Figure 3

Figure S4. Related to Figure 4

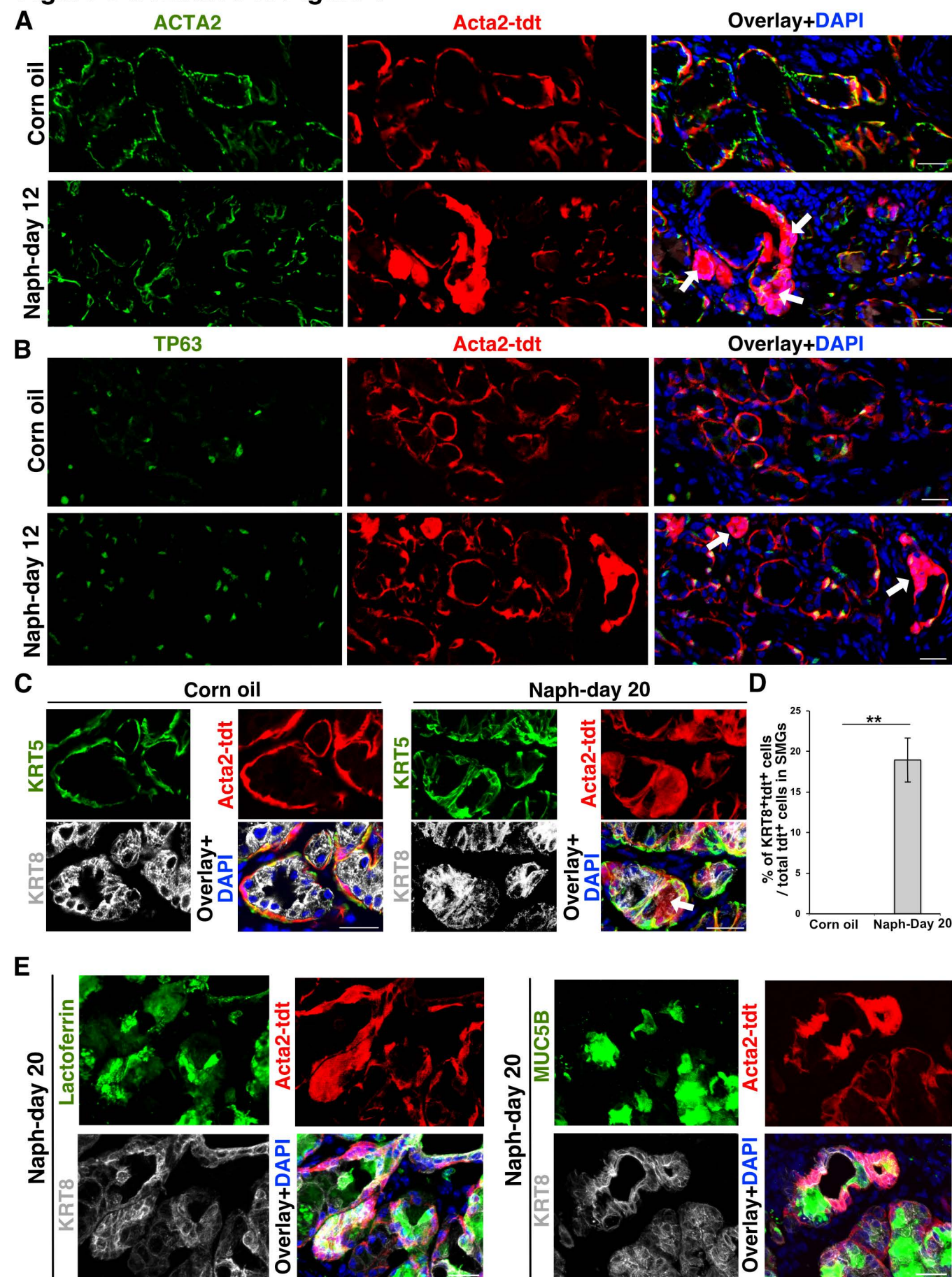


Figure S5. Related to Figure 5

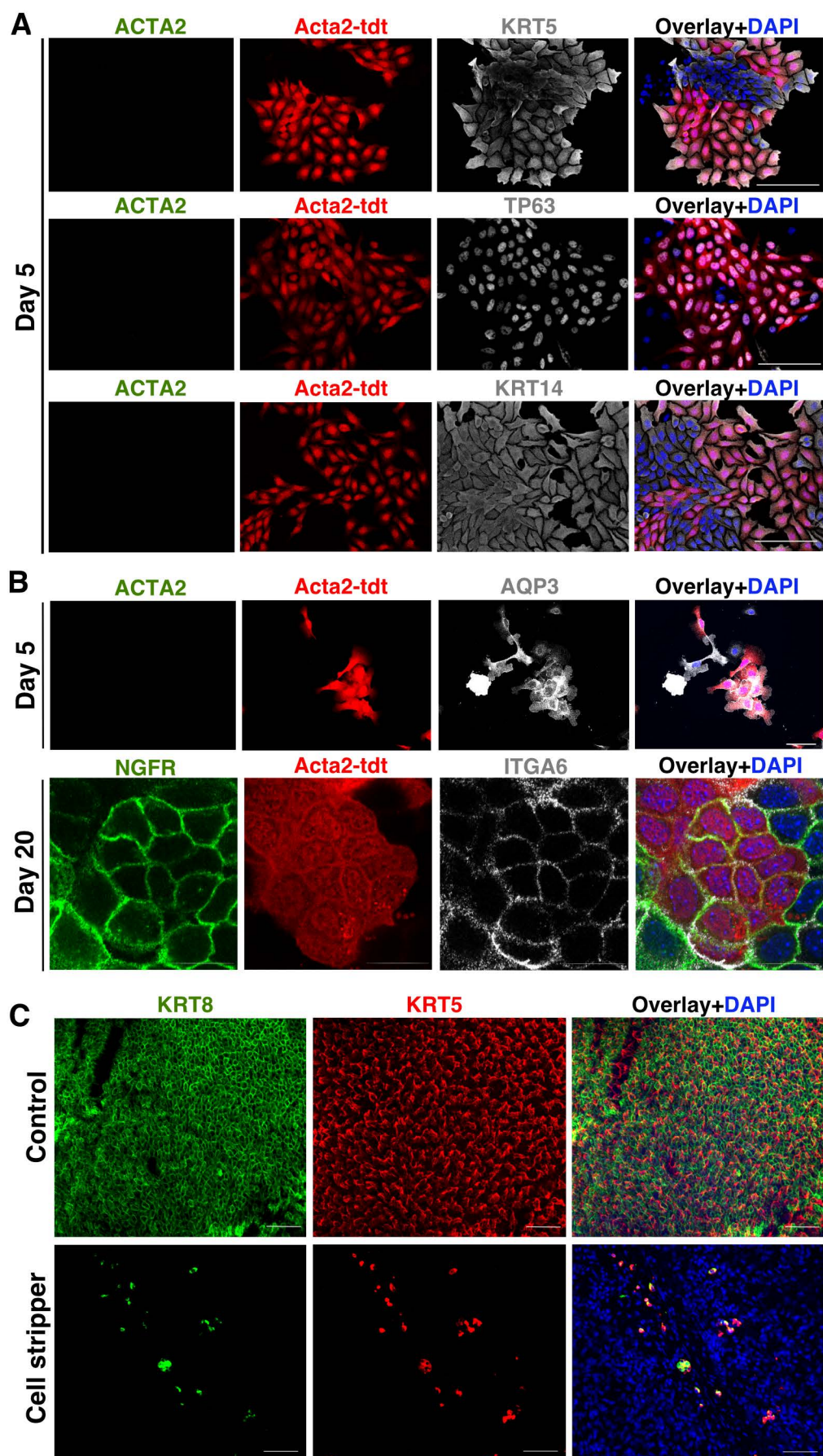
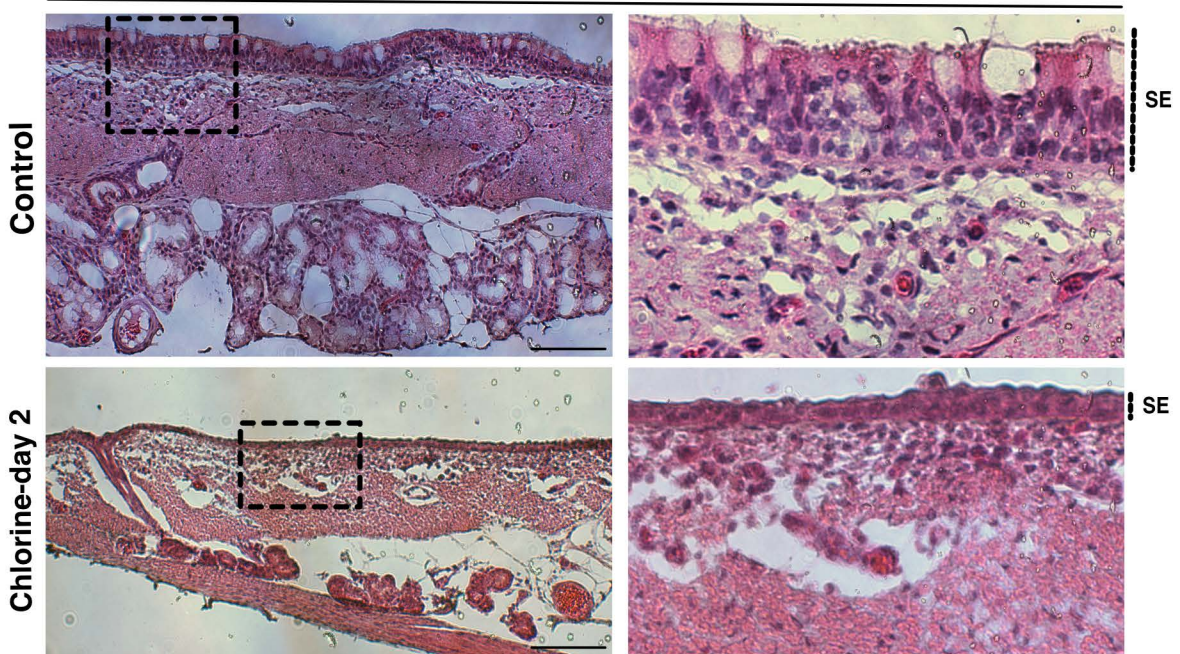


Figure S6. Related to Figure 6

A

Hematoxylin and eosin



B

SOX9 ACTA2 Ki67 Overlay+DAPI

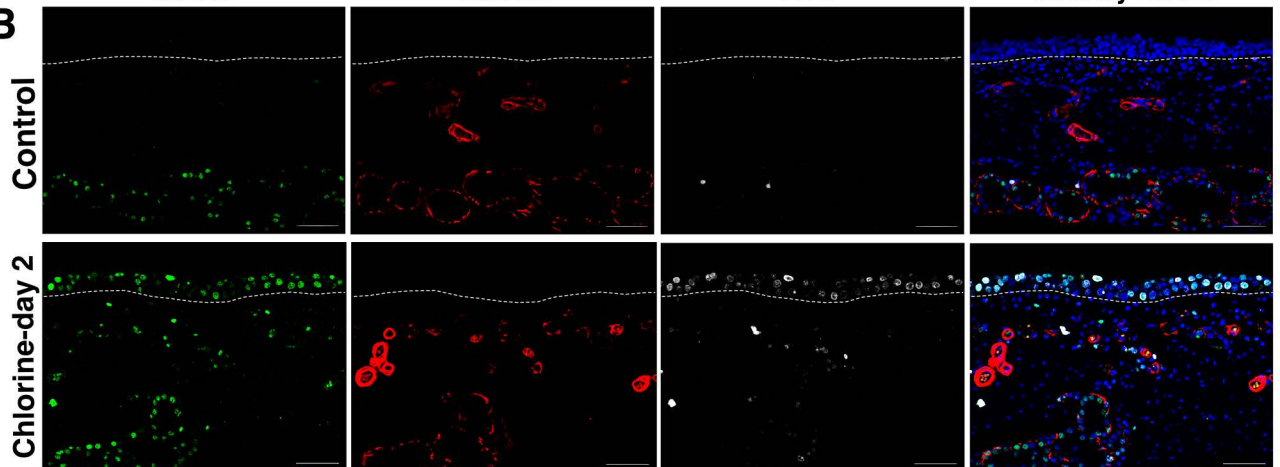
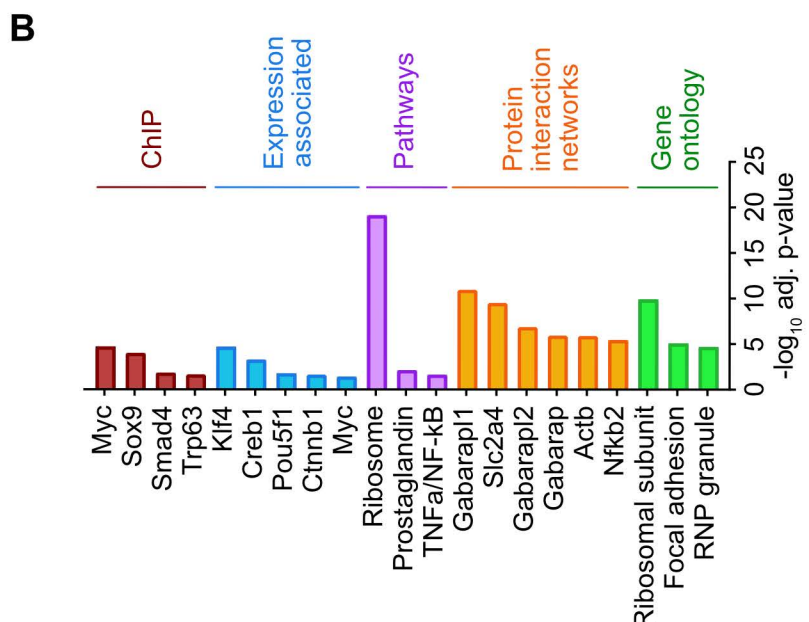
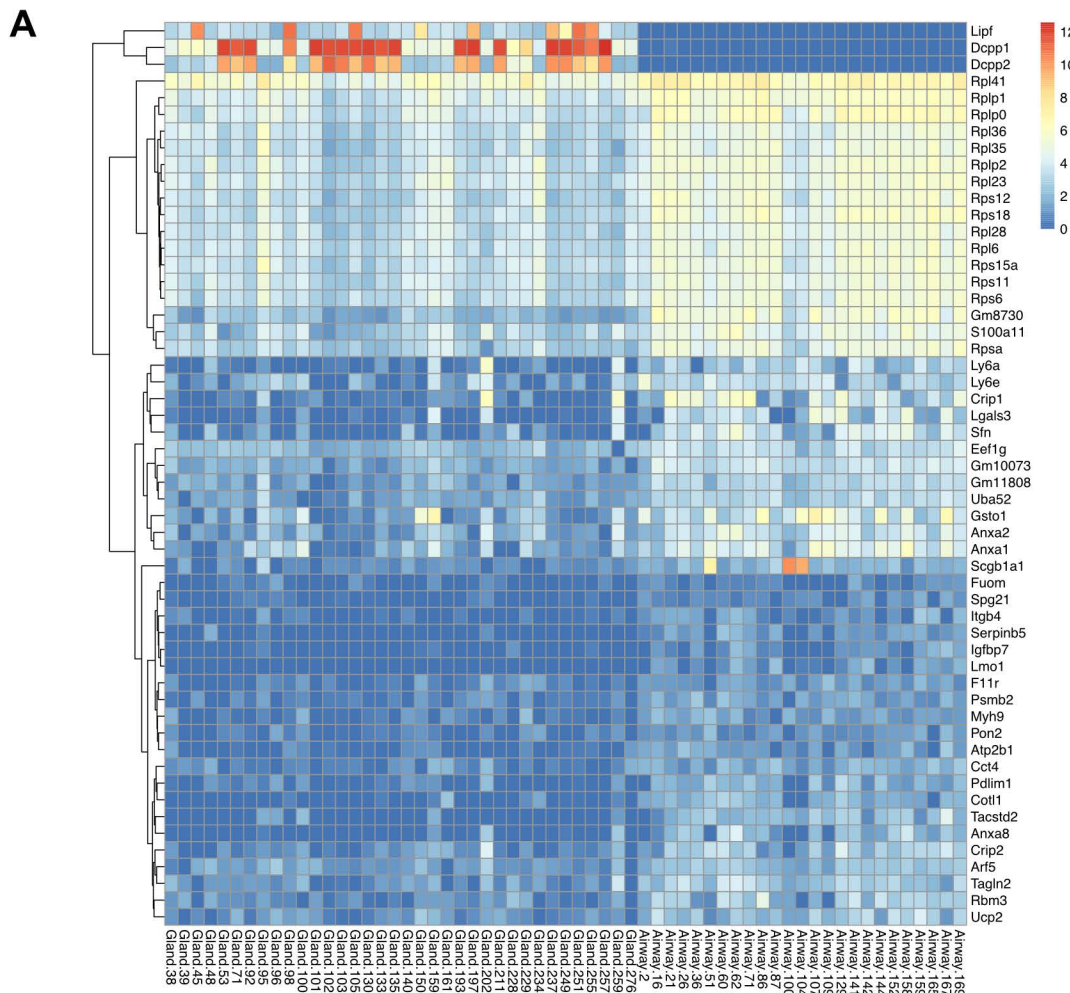


Figure S7. Related to Figure 7



Supplementary Figure legends:

Figure S1: Naphthalene-induced injury causes loss of airway SE.

(A) DAPI (blue) staining on control and naphthalene day-1 and 5 injured tracheal sections. The dashed line separates the SE cell layer from the mesenchyme. Scale bars: 50 μ m.

(B) Quantification of percent DAPI⁺ cells in SE (up to cartilage 9) in control and naphthalene (day-1 and 5) treated airways. Data shown are mean \pm SEM (n= 3; * p \leq 0.05; ** p \leq 0.01).

(C) IHC for KRT5 (green), KRT8 (red), and DAPI (blue) on longitudinal sections of airways collected from control or naphthalene injured mice. The dashed line separates the SE cell layer from the mesenchyme. Large panels were generated by aligning and stitching single pictures. Single markers shown for regions delineated by dotted box. Dotted circles indicate cartilage rings marked as C1-C3. Scale bars: 100 μ m

(D) Co-staining of ACTA2 (green), KRT14 (red), TP63 (grey) and DAPI (blue): upper panel - ACTA2 (green) and Ki67 (red); middle panel - ACTA2 (green), UEA-1 (red-mucous cell marker) and lactoferrin (grey-serous cell marker); lower panel - tracheal sections collected from control and naphthalene injured mice. Scale bar: 100 μ m

Figure S2: SMG-like cells appear in SE in multiple injury models

(A) Schematic of experimental design for sulphur dioxide (SO₂) or H1N1 PR8 infection injury models.

(B) IHC for KRT5 (red), KRT8 (grey) and DAPI (blue) on trachea sections from control, SO₂ and influenza day-1 and 3 injured mice. The dashed line separates the SE cell layer from the mesenchyme. Scale bars: 50 μ m.

(C) Quantification of percent DAPI⁺ cells in SE (up to cartilage 9) in control, SO₂ (day-1, 3 and 5) and influenza (day-1, 3 and 5) injured airways. Data shown as mean \pm SEM (n = 3; ***p* \leq 0.01).

(D) Co-staining of ACTA2 (green), SOX9 (red), Ki67 (grey), DAPI (blue) in SO₂ injured trachea. The dotted line separates the SE and mesenchyme. Large panels were generated by aligning and stitching single pictures. Scale bar: 100 μ m.

(E) Quantification of ACTA2⁺, SOX9⁺ and Ki67⁺ cells among total DAPI⁺ cells in SE of control and SO₂ injured mice. Data shown as mean \pm SEM (n=3; **p* \leq 0.05; ***p* \leq 0.01; ****p* \leq 0.001). C0-3, C3-6, and C6-9 refer to SE spanning cartilage rings between 0-3, 3-6 or 6-9 respectively. *p*- values were determined compared to controls.

(F) Quantification of ACTA2⁺, SOX9⁺ co-expressing Ki67⁺ cells in SE of control and day-5 post SO₂ injury. Data shown as mean \pm SEM (n=3; ***p* \leq 0.01; ****p* \leq 0.001). *p*- values were determined compared to controls.

(G) Co-staining of ACTA2 (green), SOX9 (red), Ki67 (grey), DAPI (blue) in influenza injured trachea. Large panels were generated by aligning and stitching single pictures. The dotted line separates the SE and mesenchyme. Scale bar: 100 μ m.

(H) Quantification of ACTA2⁺, SOX9⁺ and Ki67⁺ cells among total DAPI⁺ cells in SE of control and influenza injured mice. Data shown as mean \pm SEM (n=3; **p* \leq 0.05; ***p* \leq 0.01). C0-3, C3-6, and C6-9 refer to SE spanning cartilage rings between 0-3, 3-6 or 6-9 respectively. *p*- values were determined compared to controls.

(I) Quantification of ACTA2⁺, SOX9⁺ co-expressing Ki67⁺ cells in SE of control and day-5 post PR8 injury. Data shown as mean \pm SEM (n=3; ****p* \leq 0.001). *p*- values were determined compared to controls.

Figure S3: Sox9-expressing SMG cells contribute to the SE repair following naphthalene-induced injury.

- (A)** Representative images of Sox9-tdt SMG after tamoxifen treatment co-stained with ACTA2 and SOX9 (green) upper panel (Scale bar: 100μm) and KRT5 (green) and KRT8 (grey) lower panel. Scale bar: 50μm.
- (B)** Three months old Sox9-tdt mice received three doses of tamoxifen and were sacrificed at 13 months. Sox9-tdt (red) Tracheal sections were co-stained for KRT5 (green) and KRT8 (grey) and nuclear DAPI (blue). Scale bar: 50μm
- (C)** IHC for KRT14 (green) and Sox9-tdt (red) on airway sections from day 5 and 10 post naphthalene injury. Scale bar: 100μm.
- (D)** Co-staining of ZO-1 (green), CDH1 (grey) and Sox9-tdt (red) from control and day-5 and day-20 naphthalene injured Sox9-tdt trachea mice. Scale bar: 50μm.

Figure S4: SMG-derived ACTA2-lineage labeled MECs repair SMGs and contribute to both basal and luminal cells *in vivo* following injury

- (A)** Acta2-lineage labeling and IHC for ACTA2 (green) on control and naphthalene day 12 injured tracheal SMGs. The arrows indicate luminal Acta2-tdt lineage labeled cells in injured trachea. Scale bar: 20μm.
- (B)** Acta2-lineage labeling and IHC for basal cell marker TP63 (green) on control and naphthalene day 12 injured tracheal SMGs. The arrows indicate TP63-Acta2-tdt lineage labeled cells in injured tracheal SMGs. Scale bar: 20μm.

(C) Co-staining of KRT5 (green) and KRT8 (grey) in control or naphthalene-day 20 Acta2-tdt mice. The arrows indicate luminal cells derived from Acta2-tdt lineage labeled cells in injured trachea. Scale bar: 20 μ m.

(D) Quantification of KRT8⁺Acta2-tdt⁺ cells among total Acta2-tdt⁺ cells in SMGs in control and naphthalene day- 20 injured mice. Data shown as mean \pm SEM (n=3; ** $p \leq 0.01$).

(E) Lactoferrin (green; left panel) and Muc5B (green; right panel) co-stained with KRT8 (grey), DAPI (blue) in naphthalene injured day-20 Acta2-tdt (red) mice. Scale bar: 20 μ m

Figure S5: SMG cells culture and engraftment models.

(A) Isolated Acta2-tdt myoepithelial cells were cultured for 5 days, then fixed and stained for ACTA2 (green), KRT5, TP63, and KRT14 (grey), nuclear DAPI (blue). Scale bar: 50 μ m.

(B) Acta2-tdt cells cultured for 5 or 20 days followed by co-IHC for ACTA2 (green) and AQP3 (grey) –upper panel or NGFR (green) and ITGA6 (grey) – lower panel.

(C) KRT8 (green) and KRT5 (grey) whole mount IF on trachea treated with PBS (control) or cell stripper. Scale bar: 50 μ m

Figure S6: Chlorine gas-inhalation causes severe damage to porcine airway tissues.

(A) Hematoxylin and eosin staining on filtered air or chlorine gas administered pig airways on day- 2 post exposure. Scale bar: 100 μ m. Black box indicates magnified area shown in right panels.

(B) Co-staining of SOX9 (green), ACTA2 (red), Ki67 (grey), and DAPI (blue) in chlorine injured porcine trachea. The dotted line separates the SE and mesenchyme. Scale bar: 50 μ m

Figure S7: Single cell RNA-seq analysis identifies differentially expressed genes and pathways.

- (A)** Heatmap shows differentially expressed genes between Acta2^+ cells from homeostatic SMGs and Acta2^+ cells on SE following naphthalene-induced injury, as identified through scRNA-seq analysis.
- (B)** Enricher analysis identifies Gene Ontology terms, pathways, genomic and proteomic regulatory networks associated with differentially expressed genes between Acta2^+ cells from homeostatic SMGs and Acta2^+ cells on SE following naphthalene-induced injury.